7-2-2011

Effect of an aeroelastic film on confined subsonic cavity resonance

Melissa Carter

Melissa Carter
Candidate

Mechanical Engineering
Department

This thesis is approved, and it is acceptable in quality and form for publication:

Approved by the Thesis Committee:

C Randall Truman, Chairperson

EFFECT OF AN AEROELASTIC FILM ON CONFINED SUBSONIC CAVITY RESONANCE

by

MELISSA CARTER

B.S., MEHCANICAL ENGINEERING, UNIVERSITY OF NEW MEXICO, 2001

THESIS

Submitted in Partial Fulfillment of the
Requirements for the Degree of

Master of Science

Mechanical Engineering

The University of New Mexico
Albuquerque, New Mexico

May 2011

ACKNOWLEDGEMENTS

I acknowledge Professor C. Randall Truman; my advisor, for his guidance, long hours of editing, recommendations, and his patience.

I also thank my committee members, Dr. Peter Vorobieff, and Dr. Arsalan Razani, for their valuable recommendations.

Gratitude is extended to all at Diversified Tooling Corporation for contributing; all the materials and machining.

To my best friend, Christine Sandoval, thank you for the many years of support. Your encouragement is greatly appreciated.

To my mentor, John Ditter, thanks for praying that I pass.

To the Sandoval family for all the free meals provided to me during the months of thesis.

And finally to my mom, Mary Thomas, your love is the greatest gift of all.

Stand up, aim true, keep heart, the future looks to you, every second you throw away, every minute of every day, don't get caught in a memory, Life won't wait for you.

Ozzy Osbourne-Life Won't Wait

EFFECT OF AN AEROELASTIC FILM ON CONFINED SUBSONIC CAVITY RESONANCE

BY

MELISSA CARTER

ABSTRACT OF THESIS

Submitted in Partial Fulfillment of the
Requirements for the Degree of

Master of Science

Mechanical Engineering

The University of New Mexico
Albuquerque, New Mexico

May 2011

EFFECT OF AN AEROELASTIC FILM ON CONFINED SUBSONIC CAVITY RESONANCE

by

Melissa Carter

B.S., Mechanical Engineering, University of New Mexico, 2001

M.S., Mechanical Engineering, University of New Mexico, 2011

ABSTRACT

Two shallow three-dimensional cavities were used to study the effect on cavity resonance of an aeroelastic film placed on the wall opposite the cavity in confined (duct) flow. Flow speeds were very low subsonic with Mach number varying from 0.05 to 0.10. The cavities have length-to-depth ratios of 2.5 and 1.5, with identical depths. It was expected that the aeroelastic film in flutter would interact with acoustic signals from the cavity to enhance or inhibit cavity pressure oscillations. Two different film tensions were applied to the film to affect flutter conditions. However, the film support mechanism design did not allow flutter, and each film experienced static displacement caused by outside air pressure. Cavity sound data recorded by a microphone was compared for tests with and without the film. The effects of film tension were insignificant, primarily because the film was not in flutter. The longer cavity exhibited higher sound pressure

levels over the entire range of frequencies with an aeroelastic film present. The shorter cavity showed smaller differences, perhaps because the film is longer than the cavity. The presence of an aeroelastic film did affect the shear-layer frequencies in the cavities. For Cavity 2, higher amplitude peaks in the range of estimated resonance frequencies were observed with the film present. The results for the longer cavity indicate that a film on the opposite wall will interact with cavity pressure oscillations to affect sound pressure levels in resonance.

TABLE OF CONTENTS

LIST OF FIGURES ..... **ix**

LIST OF TABLES ..... **xii**

GLOSSARY ..... **xiii**

CHAPTER 1 INTRODUCTION **1**

1.1 Overview 1

1.2 Cavity Flow Categorization 4

1.3 Noise Cancellation 7

1.4 Membrane Dynamics 8

CHAPTER 2 EXPERIMENTAL SETUP **10**

2.1 Experimental Facility 10

2.2 Cavity Design 10

2.3 Film Tension Design 15

2.4 Measurement Equipment 18

CHAPTER 3 EXPERIMENTAL SETUP **19**

3.1 Experiments 19

3.2 Flow Settings 20

3.3 Determining Placement of Microphone 20

3.4 Confined Flow without Film 30

3.5 Determining Background Noise 34

3.6 Flutter Film Tests 38

CHAPTER 4 EFFECT OF FILM ON CAVITY RESONANCE 39

4.1 Results 39

4.2 Discussion 47

CHAPTER 5 CONCLUSION 49

5.1 Conclusion 49

5.2 Implications for Future Research 49

REFERENCES 51

LIST OF FIGURES

Figure 1. Two sinusoidal waves with the same amplitude combined in phase and out of phase. 3

Figure 2. Sketch of experimental setup; top view of wind tunnel. 4

Figure 3. Open, shallow cavity shear-layer acoustic interaction (Cattafesta, et al., 2008).6

Figure 4. Rossiter frequencies for given cavities at different Mach numbers. 12

Figure 5. Frequency response curve for Shure MC50B (www.shure.nl). The abscissa is frequency in Hz.. 14

Figure 6. Cavity 2 attached to window with bore holes for microphone insertion plugged.. 14

Figure 7. Cavity 1 mounted to the TBLG with microphone at the downstream location on the floor of the cavity.. 15

Figure 8. Film clamping assembly showing three pieces that comprise the window, the film stretched across the rectangular hole, and the tension rod (on the right) 16

Figure 9. Film tension vs. film strain.. 17

Figure 10. (a) Cavity 1 port locations and (b) Cavity 2 port locations; drawing are not to scale....21

Figure 11. Cavity 1 microphone power spectra for Mach 0.05 at ports 1, 2, and 3....22

Figure 12. Cavity 1 microphone power spectra for Mach 0.05 at ports 4, 5, and 6....23

Figure 13. Cavity 1 microphone power spectra for Mach 0.05 at ports 7-13. 23

Figure 14. Cavity 1 microphone power spectra for Mach 0.05 at ports 14-20. 24

Figure 15. Cavity 1 microphone power spectra for Mach 0.05 at ports 21-27 with close-up view of largest amplitude peaks at high frequencies... 25

Figure 16. Cavity 2 microphone power spectra for Mach 0.05 at ports 1, 2, and 3....26

Figure 17. Cavity 2 microphone power spectra for Mach 0.05 at ports 4, 5, and 6....27

Figure 18. Cavity 2 microphone power spectra for Mach 0.05 at ports 7-11. 27

Figure 19. Cavity 2 microphone power spectra for Mach 0.05 at ports 12-16. 28

Figure 20. Cavity 2 microphone power spectra for Mach 0.05 at ports 17-21 with close-up view of largest amplitude peaks at high frequencies 29

Figure 21. Cavity 1 microphone power spectra of confined flow at varying Mach numbers.....31

Figure 22. Cavity 1 microphone power spectra of confined flow at varying Mach numbers in the lower frequency range with red dashed lines indicating calculated Rossiter frequencies. 32

Figure 23. Cavity 1 microphone power spectra of confined flow at varying Mach numbers in the higher frequency range with red dashed ovals indicating peaks near resonance frequencies determined using the confinement ratio.. 32

Figure 24. Cavity 2 microphone power spectra of confined flow at varying Mach numbers... 33

Figure 25. Cavity 2 microphone power spectra of confined flow at varying Mach numbers in the lower frequency range with red dashed lines indicating calculated Rossiter frequencies.... 33

Figure 26. Cavity 2 microphone power spectra of confined flow at varying Mach numbers in the higher frequency range with red dashed ovals indicating peaks near resonance frequencies determined using the confinement ratio..... 34

Figure 27. Cavity 1 microphone power spectra (a) with noise removal and (b) without noise removal.... 36

Figure 28. Cavity 2 microphone power spectra (a) with noise removal and (b) without noise removal... 37

Figure 29. Cavity 1 microphone power spectra data at Mach 0.05 with film and without film... 41

Figure 30. Cavity 1 microphone power spectra data at Mach 0.06 with film and without film... 42

Figure 31. Cavity 1 microphone power spectra data at Mach 0.07 with film and without film. 42

Figure 32. Cavity 1 microphone power spectra data at Mach 0.08 with film and without film.... 43

Figure 33. Cavity 1 microphone power spectra data at Mach 0.09 with film and without film..... 43

Figure 34. Cavity 1 microphone power spectra data at Mach 0.10 with film and without film.....44

Figure 35. Cavity 2 microphone power spectra data at Mach 0.05 with film and without film.....44

Figure 36. Cavity 2 microphone power spectra data at Mach 0.06 with film and without film...45

Figure 37. Cavity 2 microphone power spectra data at Mach 0.07 with film and without film...45

Figure 38. Cavity 2 microphone power spectra data at Mach 0.08 with film and without film.....46

Figure 39. Cavity 2 microphone power spectra data at Mach 0.09 with film and without film.....46

Figure 40. Cavity 2 microphone power spectra data at Mach 0.10 with film and without film..47

LIST OF TABLES

Table 1. Cavity dimensions to be used in experiment.. 3

Table 2. Calculated resonant frequencies for cavity 1 and 2 in TBLG.....13

Table 3. Length-to-Depth and confinement ratios for each cavity... 19

Table 4. The required TBLG settings for the specified Mach numbers. The pitot-static pressure difference and corresponding freestream velocities are included.... 20

Table 5. Cavity 1 amplitude peaks at given frequencies. ... .40

Table 6. Cavity 2 amplitude peaks at given frequencies... 41

GLOSSARY

γ	Empirical constant determined by calibration
ε	Strain
η	Deflection
μ	Mass per unit density
σ	Stress
ω_{mn}	Angular velocity
c	Wave speed
C	Speed of sound
D	Depth of cavity
f	Frequency
f_R	Resonance frequency
H_m	Mean height
k	Ratio of vortex convection velocity to free stream velocity
K	Mode number
L	Length of the cavity
M	Mach number
n	Mode number
St	Strouhal number
T	Tension
U	Freestream velocity
W	Tunnel height

Y	Young’s modulus

CHAPTER 1

Introduction

1.1 Overview

Flows over cavities have been studied in order to control strong self-sustaining pressure oscillations that occur. These oscillations are caused by a feedback mechanism within the shear layer that impinges downstream in the cavity (Rockwell and Naudascher, 1978). These oscillations can then be amplified by the hydrodynamic affects that occur when the flow reattaches at the bottom or downstream side of the cavity (Rockwell and Naudascher, 1978). These oscillations can cause structural damage, increase drag, or produce noise (Rockwell and Naudascher, 1978). Experiments and computational studies have been done on various cavity sizes and flows (subsonic, transitional, and supersonic) using various types of flow control in order to understand the complex flow and find ways of controlling these oscillations whether they are resonant, elastic, or fluid-dynamic. Preventing these pressure oscillations may be useful in many engineering applications.

There are two types of flow control: passive and active. Passive control involves changing the geometry of the cavity and active control involves adding energy. Passive control is inexpensive and easy to apply. Active control requires a feedback loop and response time is critical. Both methods attempt to shift the shear layer preventing impingement on the wall.

Fluttering of film in low Mach numbers can help in designing optical membranes and for medical inhaler devices where the film may resonate from the cavity flow interaction so the maximum compound can be inhaled. The purpose of this experiment is to study the effects on cavity oscillations due to the interaction with a fluttering film placed on the opposite wall of the cavity. Film flutter may excite or inhibit specific sound frequencies. An open, shallow cavity was chosen because this flow is dominated by periodic pressure oscillations with fewer random oscillations (Plentovich, 1992). The cavity size was chosen to fall into the open, shallow cavity types.

The objective of this experiment is to place an elastic film on the wall opposite an open, shallow cavity flow and determine the effect on cavity resonance. An aeroelastic film was chosen as the opposite wall boundary with the idea that its flutter will interact with the acoustic signals created by the cavity flow. A 0.004 inch thick vinyl film was used as the material for the flutter film because of its high tensile strength, stability, and insulation properties. This will allow for several tests to be conducted without having to change out the film between each test. The aeroelastic boundary may enhance or dampen the acoustic signals created by the cavity flow. This enhancement or dampening of acoustic signals can be illustrated by two waves propagating towards each other, as shown in Figure 1. When two waves propagate toward each other with the same amplitude and phase, a new wave will be created with an increased amplitude and same phase. If the waves propagating towards each other have the same amplitude but the phase of one of the waves is shifted by 180° then a new wave will be created with no amplitude.

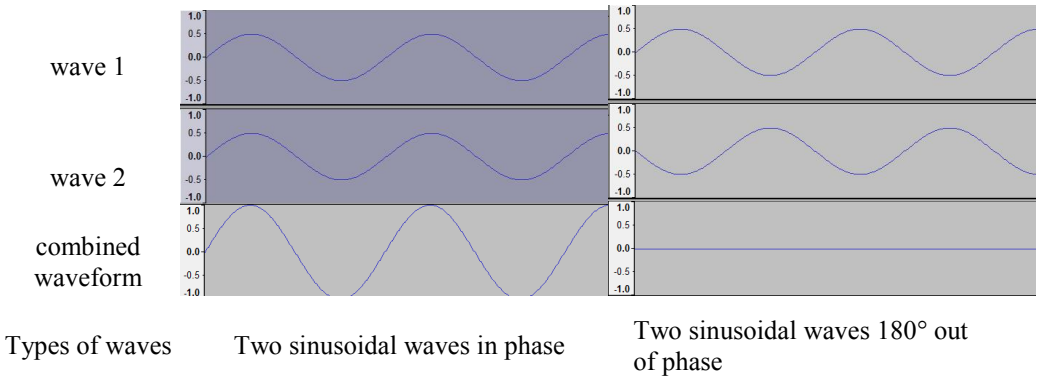

Figure 1: Two sinusoidal waves with the same amplitude combined in phase and out of phase.

For this experiment a rectangular piece of vinyl film is placed opposite the cavity from which the sound will be propagated, as shown in Figure 2. Tension in the vinyl film will be adjusted to see its effect upon cavity flow acoustics. The flutter velocity of the film will be determined by a laser Doppler vibrometer. Two different sized cavities will be studied with very low Mach numbers ranging from 0.05 to 0.1 and Reynolds numbers ranging from 10^5 to $3x10^5$. The aspect ratios for the cavities are as follows: Cavity 1 has Length-to-Depth ratio L/D=2.5 and Length-to-Width ratio L/W =2.2, Cavity 2 has L/D=1.5 and L/W=1.32. Table 1 lists the cavity parameters.

Cavity Number	Length, L (inches)	Depth, D (inches)	Width, W (inches)	L/D	L/W
1	11	4.4	5	2.5	2.2
2	6.6	4.4	5	1.5	1.32

Table 1: Cavity dimensions to be used in experiment.

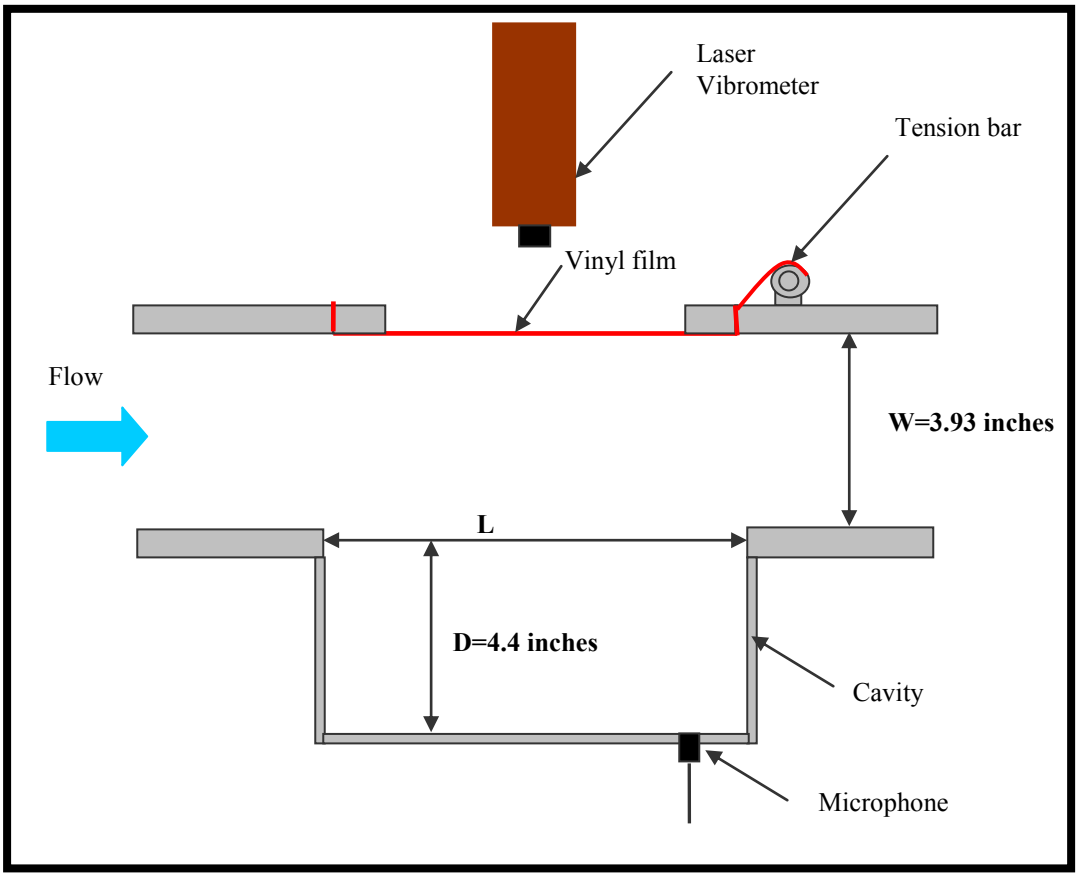

Figure 2: Sketch of experimental setup; top view of wind tunnel.

This Chapter is organized as follows: first, cavity flow categorization is discussed; second, noise suppression in subsonic open shallow cavity flows is reviewed; and finally, membrane dynamics is discussed.

1.2 Cavity flow categorization

Cavities are categorized by their aspect ratios and their reattachment zones. Open and closed cavities are defined by their reattachment zones and the Length-to-Depth ratios (L/D). In open cavity flow the boundary layer separates at the upstream corner with the shear layer reattaching at the downstream corner. Open cavities have L/D < 9 (Dix and

Bauer, 2000). A closed cavity is defined by separation at the upstream corner, impingement on the bottom of the cavity where a second separation occurs leading to stagnation at the downstream corner. Closed cavities have L/D > 13 (Dix and Bauer, 2000). A transitional cavity has an L/D in between the open and closed cavity values.

Open cavities can be further categorized as being either shallow or deep. Shallow cavities are defined by Maull and East (1963) and Kistler and Tan (1967) as cavities having a Length-to-Depth ratio L/D>0.4. Broadband noise dominates the acoustic field for shallow cavities due to more than one recirculation zone (Ahuja and Mendoza, 1995). Shallow cavities are driven in the streamwise direction by the shear layer (Rossiter 1964). Shallow cavities with L/D>0.7 can exhibit reattachment near the bottom of the cavity due to the instabilities causing the feedback loop. Deep cavities behave like acoustic resonators driven in the depth direction (Plumblee, et al., 1962).

Early cavity studies focused on the two-dimensional Rossiter (1964) analysis. More recently three-dimensional analysis (Faure, et al., 2007) has been used to better understand hydrodynamic effects in subsonic flows. Three-dimensional flows are categorized by their Length-to-Width ratio (L/W). For L/W < 1, the three-dimensional effects are not significant (Tam and Block, 1978). The difference in three-dimensional and two-dimensional flows is the reduction in far field broadband noises in the latter.

The Rossiter (1964) semi-empirical formula evaluates the dimensionless frequency, or Strouhal number, as:

$$St = \frac{fL}{U} = \frac{n - \gamma}{1/k - M}, \quad n=1, 2, 3, \ldots. \tag{1.1}$$

where n is the mode number 1,2,3, …; k, the ratio of vortex convection velocity to free stream velocity, is nearly universal at k= 0.57; M is Mach number; and γ is an empirical constant determined by calibrating to experimental data for the type of cavity (γ=0.25 for sharp edges and rectangular cavities studied herein). Figure 3 shows the mechanism of acoustic interaction with the shear layer in these types of cavities.

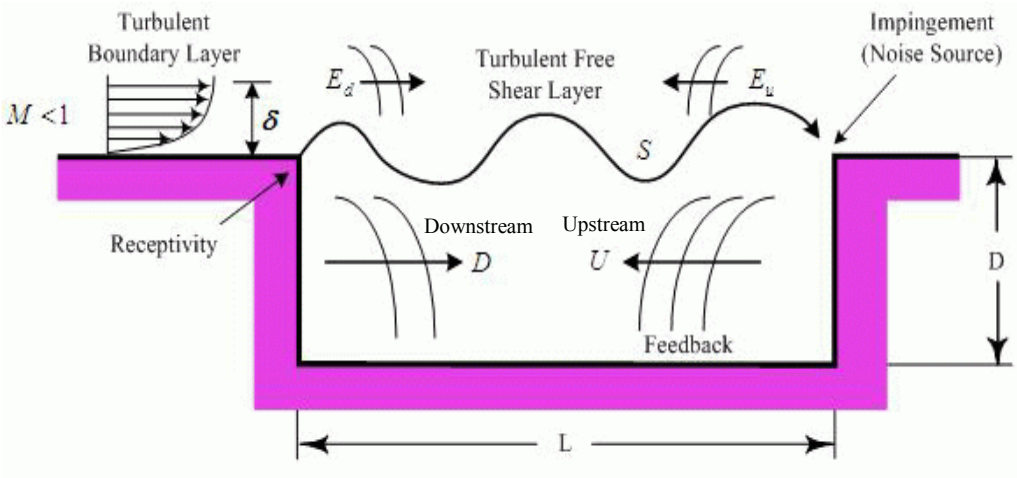

Figure 3: Open, shallow cavity shear-layer acoustic interaction. (Cattafesta, et al., 2008)

In subsonic flows with Mach < 0.3, the majority of the Rossiter modes are stable. This was found experimentally by Rowley, et al. (2002, 2005) and computationally by the Alvarez-Kerschen-Tumin approach (Alvarez, et al., 2004). These are the types of flows used in the current research.

An experimental study of confined flow was done experimentally by Ziada, et al. (2003) who moved a flow channel wall to change the effective cavity depth to determine the effects of reflections. They found that reflections of shear layer disturbances from the opposite tunnel wall promoted resonant frequencies in the cavity flow. Interactions were strongest between the first resonance mode and the first few fundamental modes of shear layer oscillations at low Mach numbers ($0.1 \leq M \leq 0.3$) compared to unconfined flow cases. The onset of resonance can be determined in terms of a mean height:

$$H_m = V + \text{Ɔ}/2 \tag{1.2}$$

where W is the width of the flow channel (Figure 2) and D is the depth of the cavity. Ziada, et al. (2003) suggested an approximate estimate for the resonance frequencies:

$$f_R = \frac{KC}{2H_m}, \quad K = 1, 2, 3 \ldots \tag{1.3}$$

where K is the mode number and C is the speed of sound.

1.3 Noise Cancellation

Noise cancellation in open cavity flows at low Mach number has been performed experimentally using both passive and active methods (Cattafesta, et al., 2008). Passive control does not add energy to the flow but only changes the flow such as modification of geometry. Active flow control adds energy to the flow through excitation or forcing. Active control is further described as closed-loop and open-loop. Closed loop refers to using some type of measurement as feedback to the control system. Open loop does not have feedback. The following will give a review of cavity control with Mach numbers below 0.3 with passive and active open control since this is what was studied in our experiment. Sarohia and Massier (1977) added steady flow injection at the upstream

corner of the cavity and found that large flow rates were needed to stabilize the flow oscillations. Cattafesta et al. (2008) used piezoelectric flaps along the upstream corner to control and successfully suppress the oscillations. Lamp and Chokani (1997) used rotary valves to produce oscillatory blowing upstream at frequencies of 750Hz. This reduced resonance tone amplitude by 10dB but new tones appeared.

1.4 Membrane Dynamics

Membranes are used in many applications including pressure transducers, computer chips, and musical instruments. A drum is an example of a musical instrument where one end of a hollow cylinder is covered by skin that is held by tension screws that can be adjusted to produce various pitches. Another example is a condenser microphone, which consists of a diaphragm held in tension over a capacitive plate. The gap between the diaphragm and the capacitive plate is modeled such that it behaves as a damped Helmholtz resonator which enhances the effective bandwidth.

Membrane vibration can be described by the wave equation (Blackstock 2000:229). The wave equation for the displacement η(x,y,t) of a rectangular membrane with length L and width W is:

$$\nabla \eta - \frac{1}{c^2}\eta_{..} = 0 \qquad (1.4)$$

where c, the wave speed on the membrane, is given by:

$$c = \sqrt{\frac{T_l}{\varsigma}} \qquad (1.5)$$

based on T_l, the tension per unit length, and ς, the mass per unit area. The normal-mode solutions can be determined by applying the initial and boundary conditions. This experiment will have two clamped ends and will therefore act similar to a two-dimensional string. The velocity of the fluttering film will be determined experimentally using a laser Doppler vibrometer.

CHAPTER 2

Experimental Setup

2.1 Experimental Facility

The experiment was conducted in a small turbulent boundary layer generator (TBLG) designed by Boeing and located at University of New Mexico. The tunnel consists of an inlet, settling chamber, contraction contour, test section, and diffuser. The inlet is shaped like a bellmouth to allow for smooth flow transition, then into honeycomb for flow straightening. The settling chamber consists of three screens that decrease in size from upstream to downstream to break up large eddies allowing for smooth flow through the chamber. The contraction contour was designed to smoothly increase the flow velocity into the test section without flow separation in the boundary layer. The test section is a constant-area rectangular duct 50 cm high, 10 cm wide, and 3.05 meters in length. The test section has two 35 cm diameter windows and four 10 cm diameter windows which sit flush to the interior walls in the test section. The exit diffuser has 15.2° total angle and three splitter plates were used to reduce the effective angle without lengthening the diffuser. The diffuser cross-sectional area is converted to circular by means of a sheet metal section connected to a flexible accordion duct to isolate vibrations from the fan motor. The blower squirrel cage is powered by a 5 h.p. motor.

2.2 Cavity Design

Two different sized cavities were designed from ¼" thick acrylic plate. The rectangular cavities were formed from pieces that were glued and sealed. The cavities were then

mounted with an o-ring on an acrylic window with a rectangular cavity cutout. The cavity sizes were chosen such that they are considered open, shallow cavities which include three-dimensional effects. Recall that an open cavity is defined by L/D < 9 with boundary layer separation at the leading corner and the shear layer reattaching at the downstream corner. A shallow cavity with L/D >0.4, has a reattachment zone at the bottom of the cavity. For L/W >1, the flow is three-dimensional. The cavities will be denoted as Cavity 1 and Cavity 2. Cavity 1 has dimensions 11 in x 5 in x 4.4 in (L x W x D), giving L/D=2.5 and L/W= 2.2. Cavity 2 has dimensions 6.6 in x 5 in x 4.4 in, giving L/D=1.5 and L/W=1.32. Each cavity had a series of bore holes on all sides for placement of a microphone. The sizes of the holes were determined after selection of the microphone.

The Rossiter or shear-layer frequencies given by Equation 1.1 and the resonant frequencies given by Equation 1.3 were calculated in order to determine the frequency range that must be measured. For the experimental tests the Mach number will vary from 0.05 to 0.10. Figure 4 shows the Rossiter frequencies versus Mach number for the two cavities.

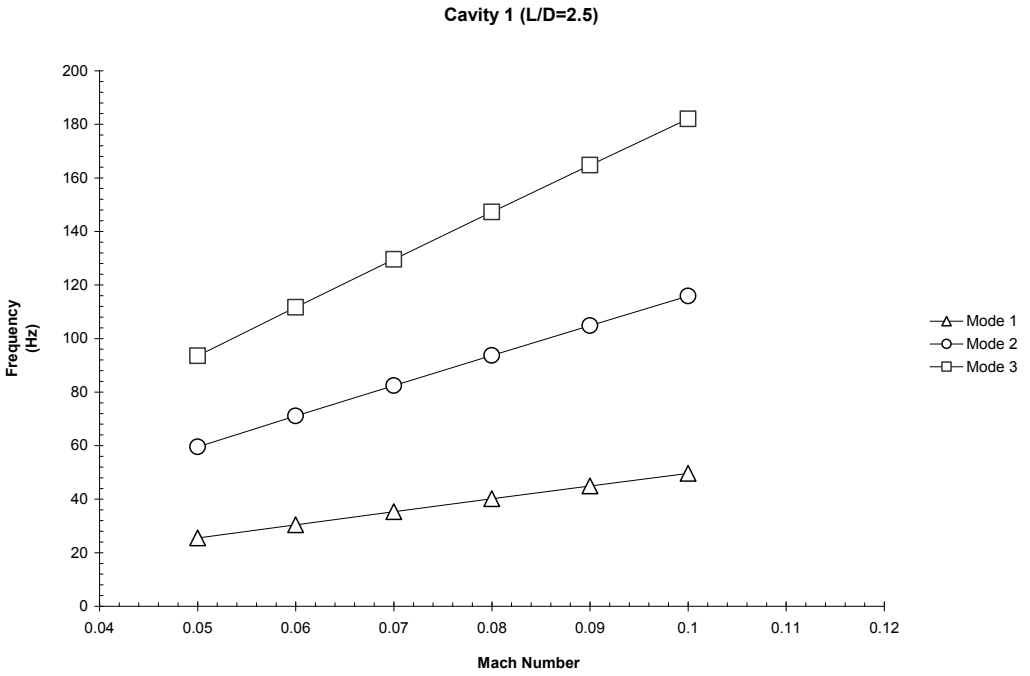

(a)

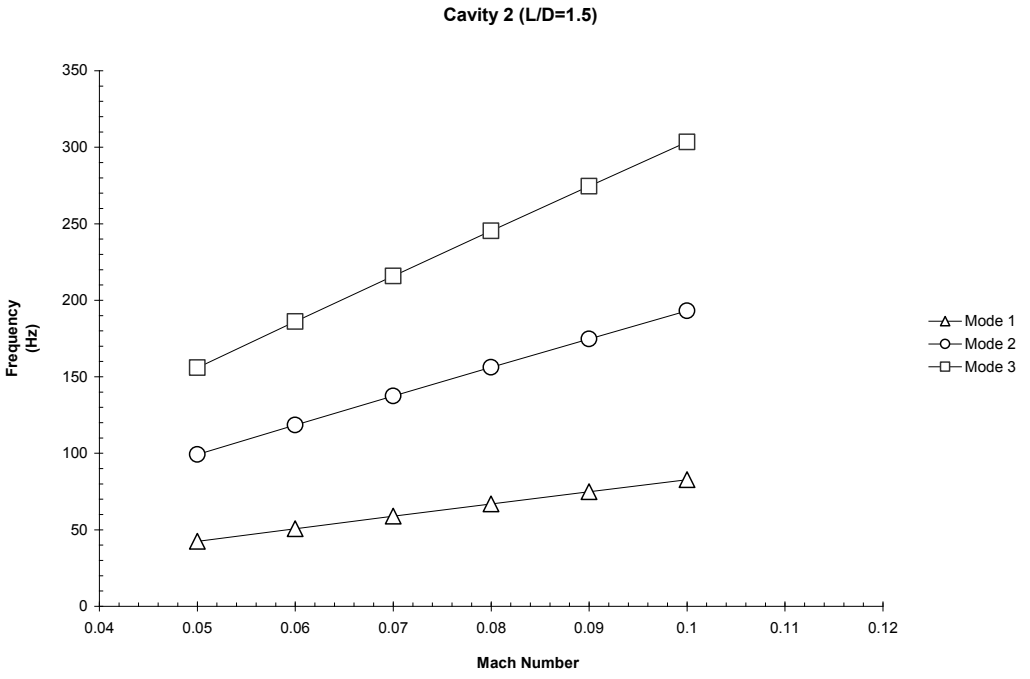

(b)

Figure 4: Rossiter frequencies for given cavities at different Mach numbers.

Table 2 shows the calculated resonance frequencies based on the mean height from Ziada, et al. (2003). Since both cavities have the same depth and flow channel width does not change, H_m= 6.14 inches for both cavities. Since cavity length does not affect the resonance modes, they are identical for both cavities. However, the Rossiter (or shear-layer) mode that interacts with a resonance mode will depend on the L/D for the cavity.

Resonance Mode	Frequency (Hz)
mode 1	1100
mode 2	2200
mode 3	3300

Table 2: Calculated resonant frequencies for cavities 1 and 2 in TBLG.

To measure the sound, or pressure amplitude and phase, a Shure omnidirectional MC50B sub-mini Lavalier microphone was selected to encompass the required frequency range. Its frequency response is shown in Figure 5. In the expected frequency range 25 Hz to 4 kHz, the performance is nearly flat, and the microphone can be expected to provide accurate representation of cavity oscillations. The diameter of the microphone is 0.23 inches. A cap (0.312 inch outer diameter) was made for the microphone to protect it and allow for tight easy insertion into the base holes in the cavity walls.

With the microphone selected the size of the holes to be placed along the cavity walls was determined. Holes placed along the centerline of each side of the cavities were 0.3281 in diameter by 0.2 in deep for the outer hole. An inner hole 0.25 inches in diameter was bored in each port so that the microphone could be placed flush to the inner wall of the cavity. The ports are 1 inch apart from center to center. To ensure that the microphone and plugs were sealed, O-rings were used. Plugs were needed in all the

holes except for where the microphone was placed. The aluminum plugs had 0.312 in diameter and length of 0.75 inch for easy removal as shown in Figure 6 for Cavity 2. Figure 7 shows Cavity 1 mounted to the TBLG with the microphone inserted into the downstream hole on the cavity floor.

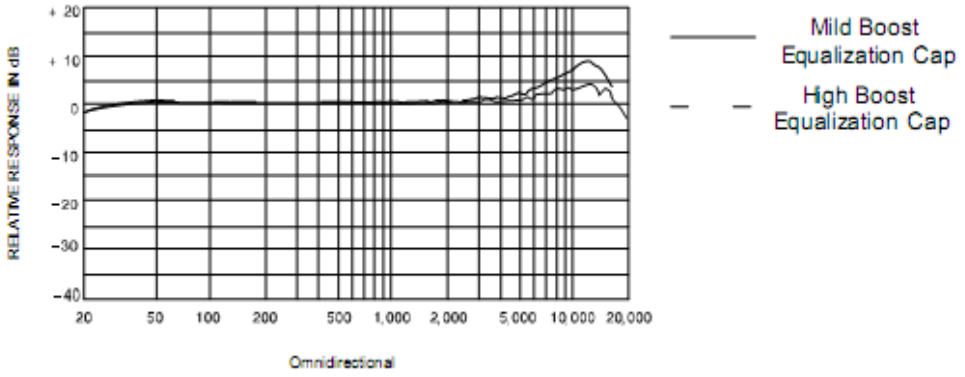

Figure 5: Frequency response curve for Shure MC50B (www.shure.nl). The abscissa is frequency in Hz.

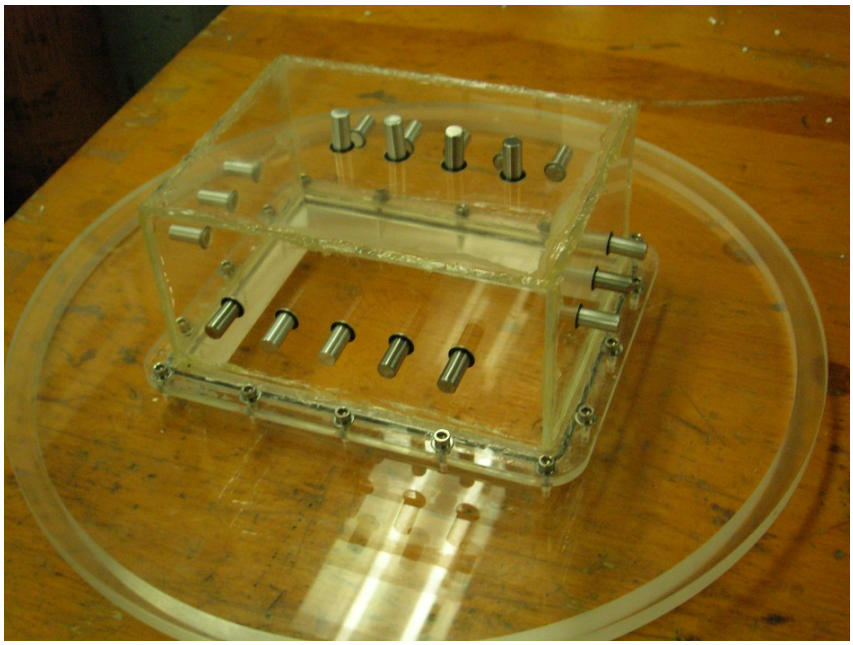

Figure 6: Cavity 2 attached to window with bore holes for microphone insertion plugged.

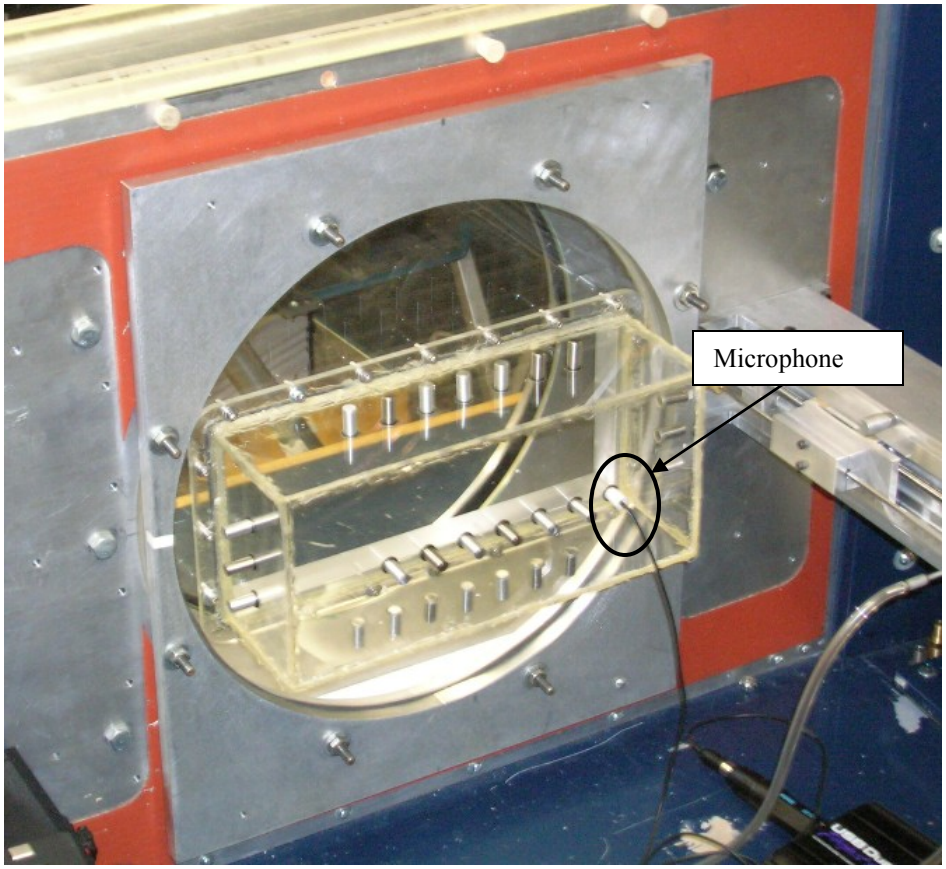

Figure 7: Cavity 1 mounted to the TBLG with microphone at the downstream location on the floor of the cavity.

2.3 Film Tension Design

The film was placed on the tunnel wall opposite the cavity and was mounted on an assembly that filled the mirror port. An acrylic window was made with a rectangular hole 7 inches (streamwise) by 5 inches (spanwise). The acrylic window along the streamwise direction was split into three pieces to allow for the film to be clamped under tension. Figure 8 shows the disassembled clamping mechanism for the film. A tension rod was attached on the outside of the window along the spanwise (vertical) direction. The tension rod is a 0.5 inch rod with 1 in knobs on each end. The rod mount includes

set screws that lock the rod in place at the desired tension. One end of the film was taped to and rolled up on the rod while the other end of the film was clamped down.

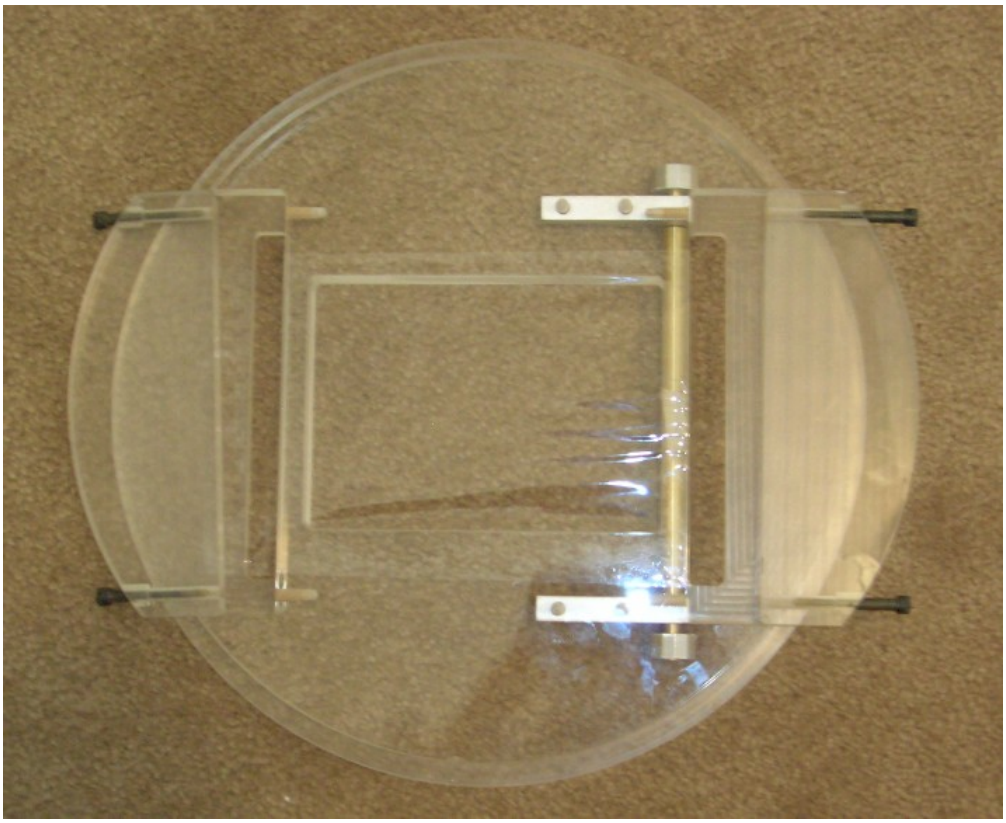

Figure 8: Film clamping assembly showing three pieces that comprise the window, the film stretched across the rectangular hole, and the tension rod (on the right).

In two sets of tests the film will be under tension and in one set it will not. The film is rolled onto the tension rod and the stretched length is measured. Since the film properties were not available, polyester film properties were used including Young's Modulus Y= 652 psi. (Petfilm®, http://www.m-petfilm.com).

Film tension is normal stress times film cross-sectional area

$$T = \sigma \tag{2.1}$$

Normal stress is Young's modulus times strain

$$\sigma = {}^{\prime}\varepsilon \tag{2.2}$$

where strain is the change in length per length

$$\varepsilon = \frac{\Lambda}{L} \tag{2.3}$$

Thus the tension is:

$$T = \frac{{}^{\mathrm{v}}\Delta \ A}{L} \tag{2.4}$$

Film area is calculated as 7 in length times 0.004 in thickness. Figure 9 shows required tension versus strain. The tensions selected for this experiment are Tension 1= 0.1 lbf and Tension 2= 0.45 lbf.

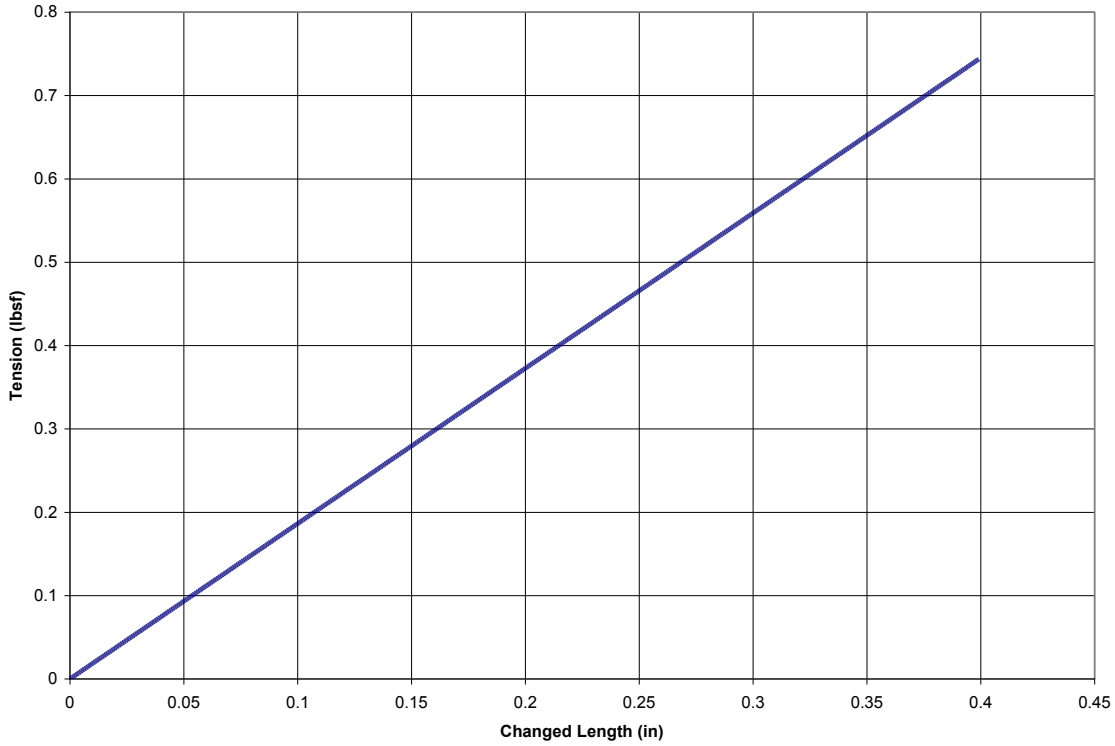

Figure 9: Film tension vs. film strain.

2.4 Measurement Equipment

The following equipment and instruments were used to record the data. A Series 160 stainless steel 1/8" diameter Dwyer® pitot tube was used to measure the freestream velocity. The pitot tube was attached to an MKS Baratron Type 223B Pressure Transducer. This transducer had a digital readout and the value was recorded manually. A MC50B Shure omnidirectional condenser microphone was connected to an ART USB Dual Pre 2 Channel Preamp then connected to a laptop computer. The software package Audacity ® (freeware; http://audacity.sourceforge.net/) used to record and edit audio signals was triggered manually to record. To measure the deflections of the vinyl film a Polytec OFV 302 vibrometer was used. The vibrometer signal was collected by a Lecroy 9304A Oscilloscope and the data was recorded onto a floppy disc.

CHAPTER 3

Experimental Tests

3.1 Experiments

The cavities were tested at the lowest Mach number with the microphone at each port to determine the placement of the microphone for the rests of the tests. To determine the optimum placement of the microphone, frequency spectra will be evaluated based on the highest peak near the calculated resonance modes. Once this was determined the cavities were tested at each Mach number with an opposing window (no film) to verify the calculated resonance modes and the Rossiter modes. The window with film clamping mechanism was then put in place and tests for each cavity were performed with varying Mach numbers at different tensions. The flutter velocity of the film was recorded with the laser Doppler vibrometer to characterize film flutter. Since cavity length is an important parameter in the shear-layer modes and depth is important in the resonance modes, the Length-to-Depth and confinement ratios (H_m/L) are given in Table 3 for each cavity.

Cavity Number	L/D	H_m/L
1	2.5	0.928
2	1.5	1.393

Table 3: Length-to-depth and confinement ratios for each cavity.

3.2 Flow Settings

Tests were run without cavities or tensioned film to determine the wind tunnel control settings necessary to produce the Mach numbers 0.05 to 0.10 in 0.01 increments. Three tests at each Mach number were performed using the Pitot probe to ensure consistency and that each cavity was leak proof. The velocities were calculated using the Air velocity calculator that came the Dwyer pitot tube. Table 4 shows the velocities and Mach numbers measured from with the pitot probe.

Velcoity calculated from Air Velocity Calculator (Dwyer) The density of air 0.062 lbs/ft^3				
TBLG Setting	**ΔP (In H_2O)**	**Velocity (ft/min)**	**Velocity (ft/s)**	**Mach Number**
26.2	0.57	3350	55.8	0.049
31.2	0.83	4025	67.0	0.059
36.2	1.15	4750	79.1	0.070
41.2	1.5	5400	90	0.079
45.2	1.83	6050	100.8	0.089
51.2	2.35	6800	113.3	0.10

Table 4: The required TBLG settings for the specified Mach numbers. The pitot-static pressure difference and corresponding freestream velocities are included.

3. 3 Determining Placement of Microphone

Each cavity was placed on the tunnel with an acrylic window replacing the film tension mechanism. Acoustic data was collected with the microphone in one port at a time, scanning the entire cavity at Mach 0.05. The purpose was to determine the optimal location of the microphone to be used for the remaining tests. The criteria to determine this will be based on the highest amplitude at frequencies corresponding to the first resonance mode. All ports were plugged and the microphone was placed in port 1, as shown in Figure 10. Each test was recorded for 3 seconds using Audacity® software with

the highest sample rate of 96000 Hz. Since the highest acoustic frequency of interest is approximately 3300 Hz, this sampling rate should minimize aliasing. The microphone was moved to port 2, with port 1 plugged, and the test repeated. This continued until data was recorded with the microphone in each port. Port 1 is located on the downstream wall of each cavity. Figure 10 shows port numbers for Cavity 1 and for Cavity 2, with flow from left to right.

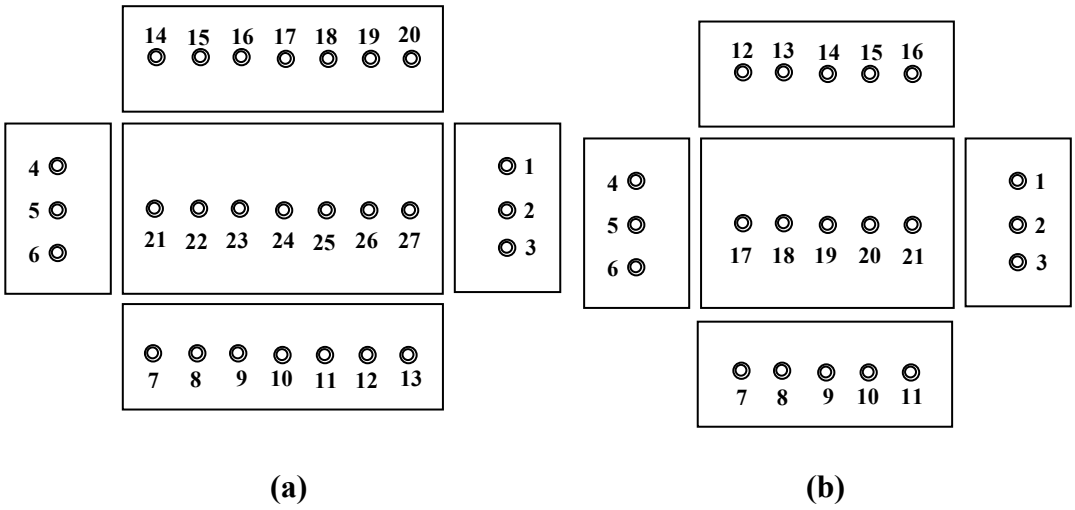

Figure 10: (a) Cavity 1 port locations and (b) Cavity 2 port locations drawing are not to scale.

The acoustic power spectra was extracted from Audacity® and opened in Excel to compare results. The results were plotted together for each wall of the cavity. For example; ports 1, 2, and 3 make up one side and were plotted together. Cavity 1 (L/D=2.5) results are shown in Figures 11-15. Although ports 1-6 showed higher amplitudes in the lower frequency range they did not meet the criteria of having high peaks in the higher frequency range and were eliminated as candidates. The location with the highest amplitudes in the frequency range above 1 kHz can be seen in Figure 15

as ports 26 and 27, downstream on the cavity floor. Other ports on the cavity floor (namely, 22 or 25) showed significant peaks at approximately 500 Hz. Figure 15 includes a close-up view of the amplitudes for frequencies from about 500 Hz to 1500Hz. Port 27, downstream on the floor of the cavity, was chosen as the microphone location since it showed the largest amplitudes in the frequency range greater than 1 kHz where resonance is expected to occur.

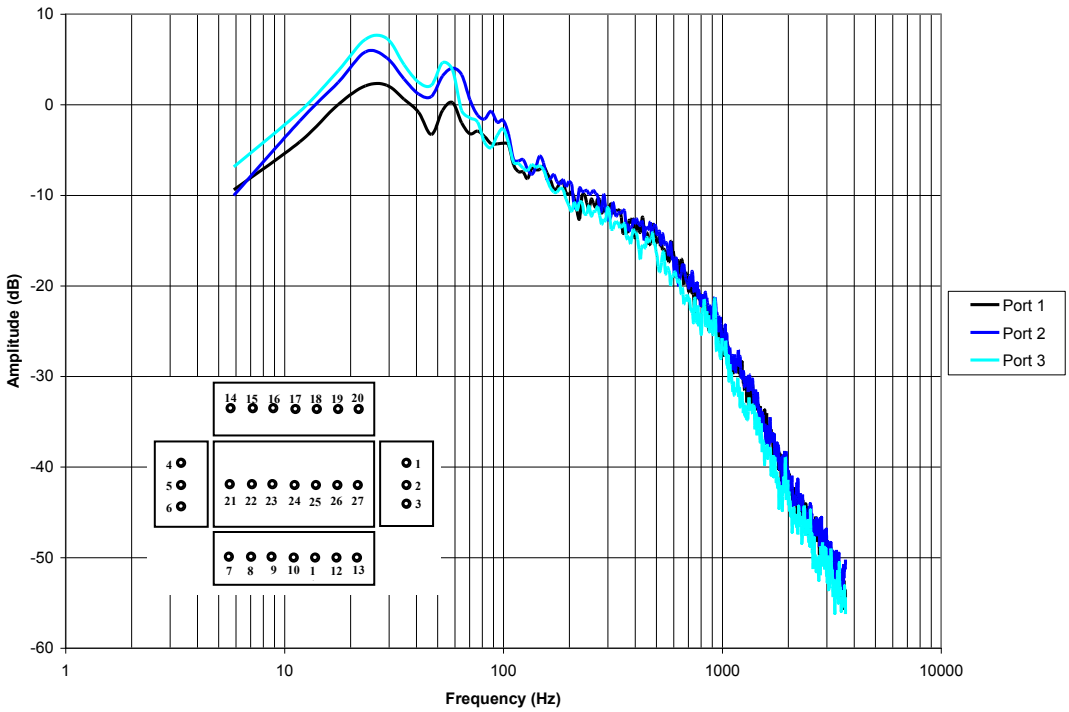

Figure 11: Cavity 1 microphone power spectra for Mach 0.05 at ports 1, 2, and 3.

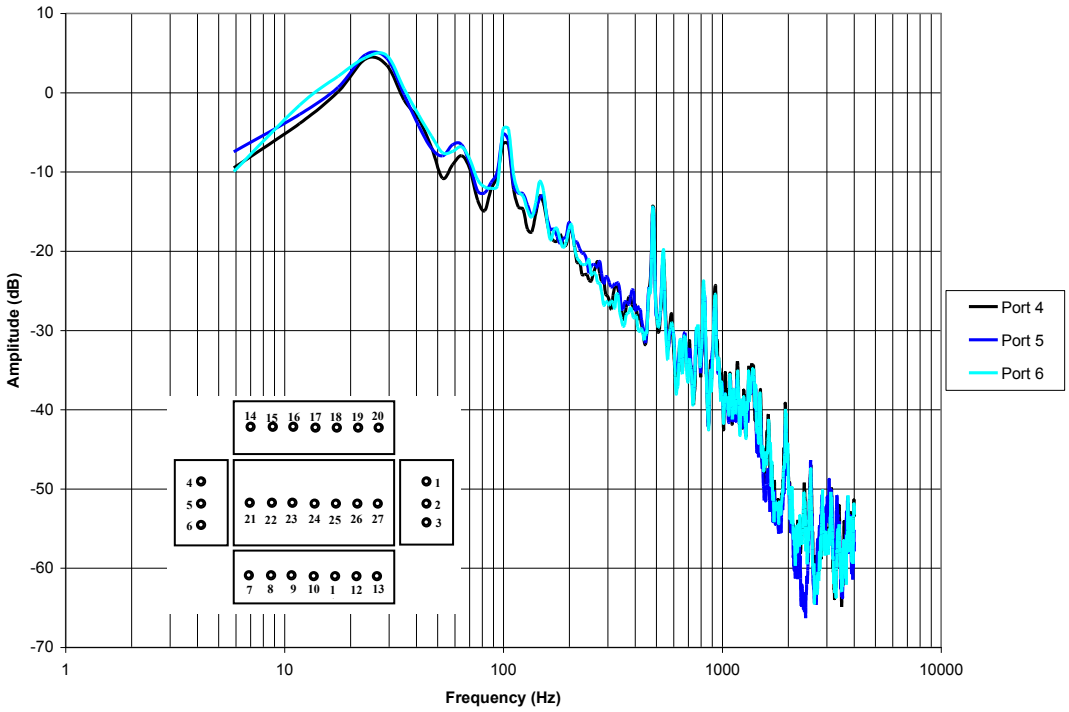

Figure 12: Cavity 1 microphone power spectra for Mach 0.05 at ports 4, 5, and 6.

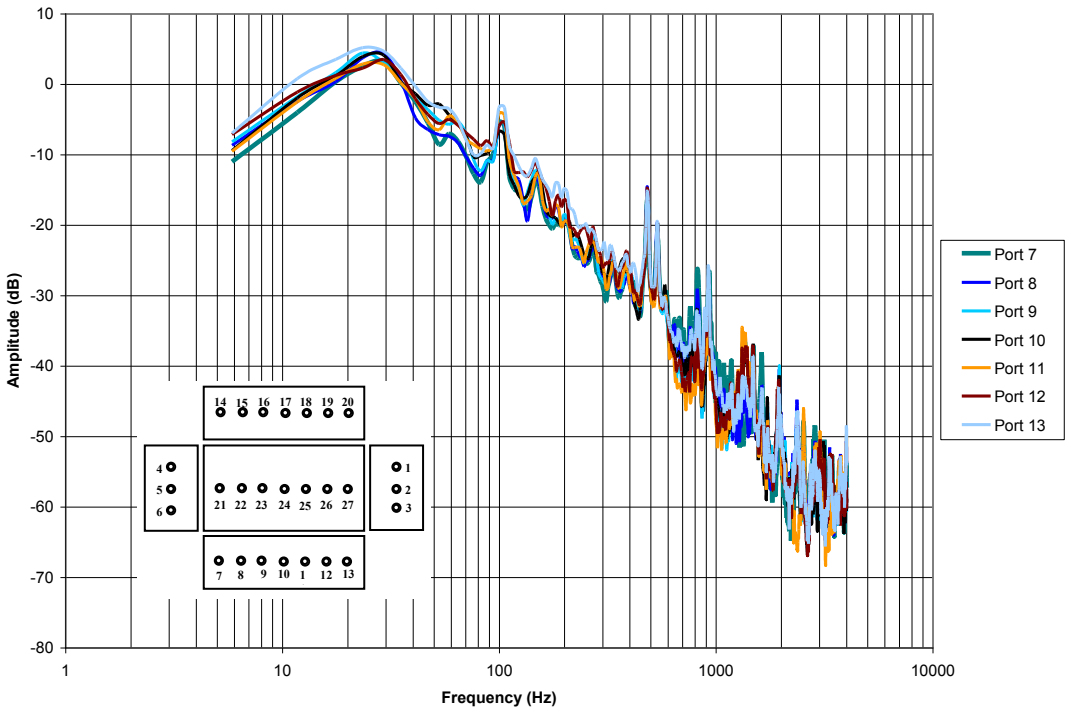

Figure 13: Cavity 1 microphone power spectra for Mach 0.05 at ports 7-13.

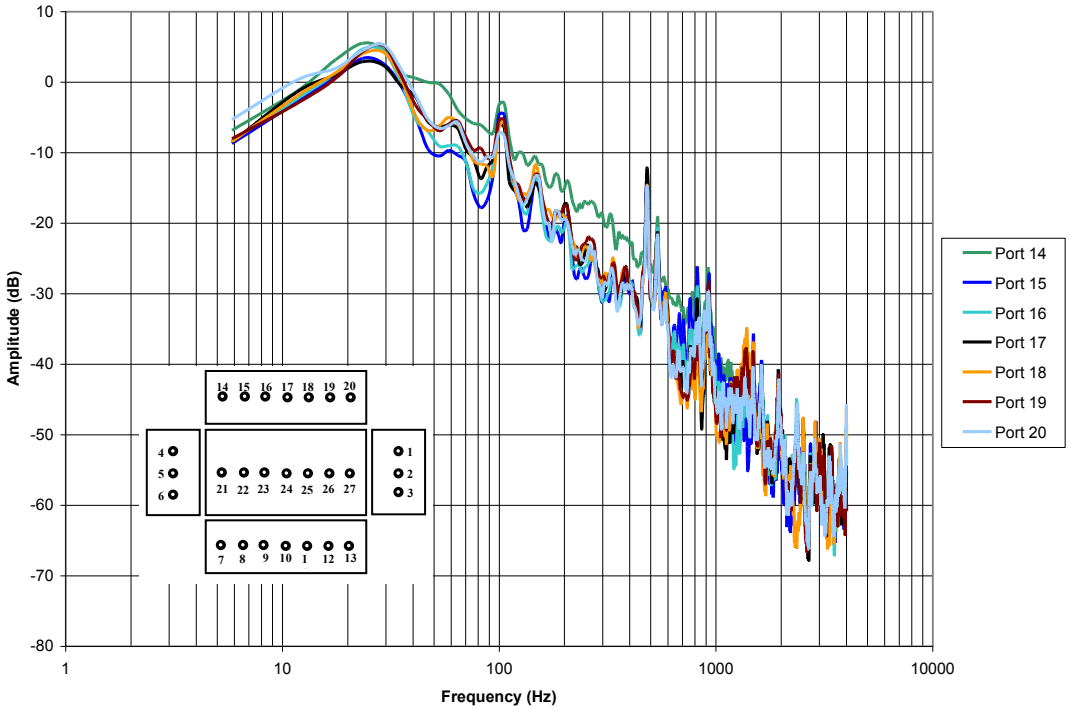

Figure 14: Cavity 1 microphone power spectra for Mach 0.05 at ports 14-20.

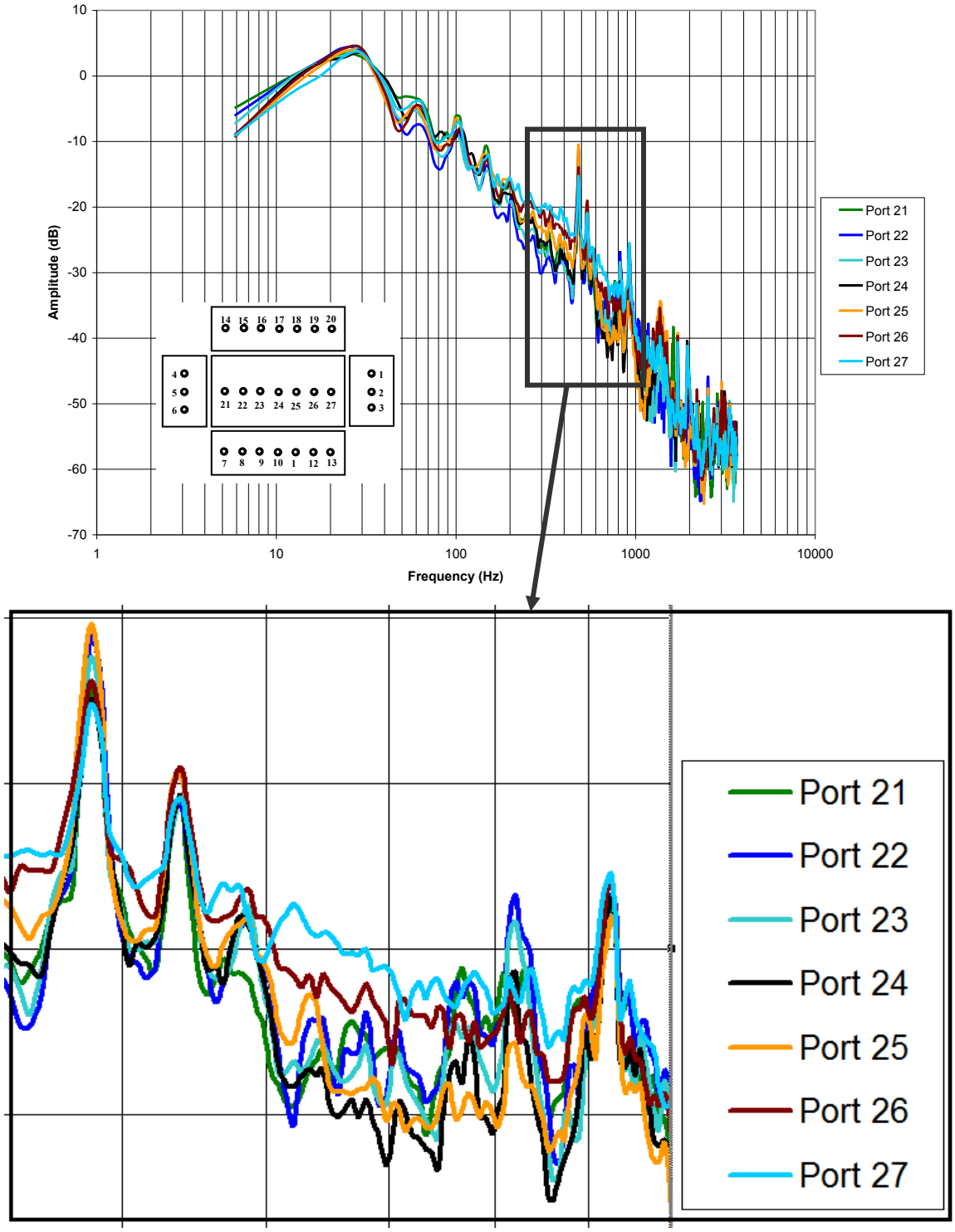

Figure 15: Cavity 1 microphone power spectra for Mach 0.05 at ports 21-27 with close-up view of largest amplitude peaks at high frequencies.

Cavity 2 (L/D=1.5) results are shown in Figures 16-20. All microphone locations exhibit high amplitudes in the high frequency range. The highest peaks at approximately 500 Hz occurred in ports 17 and 18 (upstream end of the floor) as shown in Figure 20. Since the difference in these peaks was no greater than 3 dB, port 21 was chosen as the location for the microphone. This is the same location as selected for Cavity 1, the downstream end on the floor of the cavity.

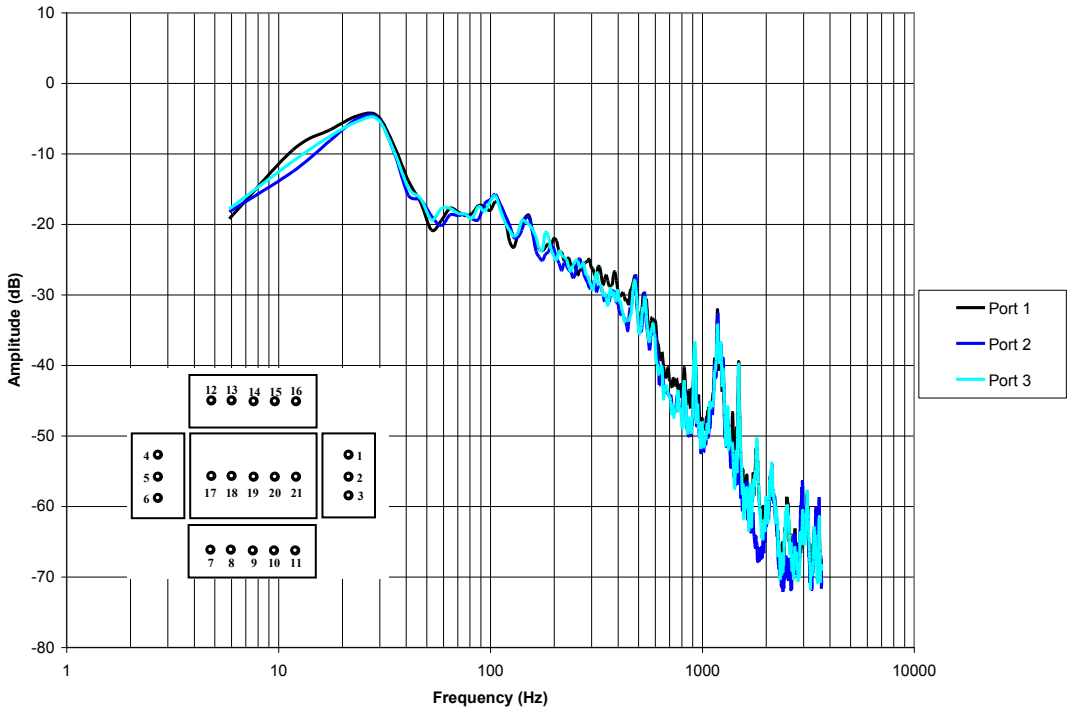

Figure 16: Cavity 2 microphone power spectra for Mach 0.05 at ports 1, 2, and 3.

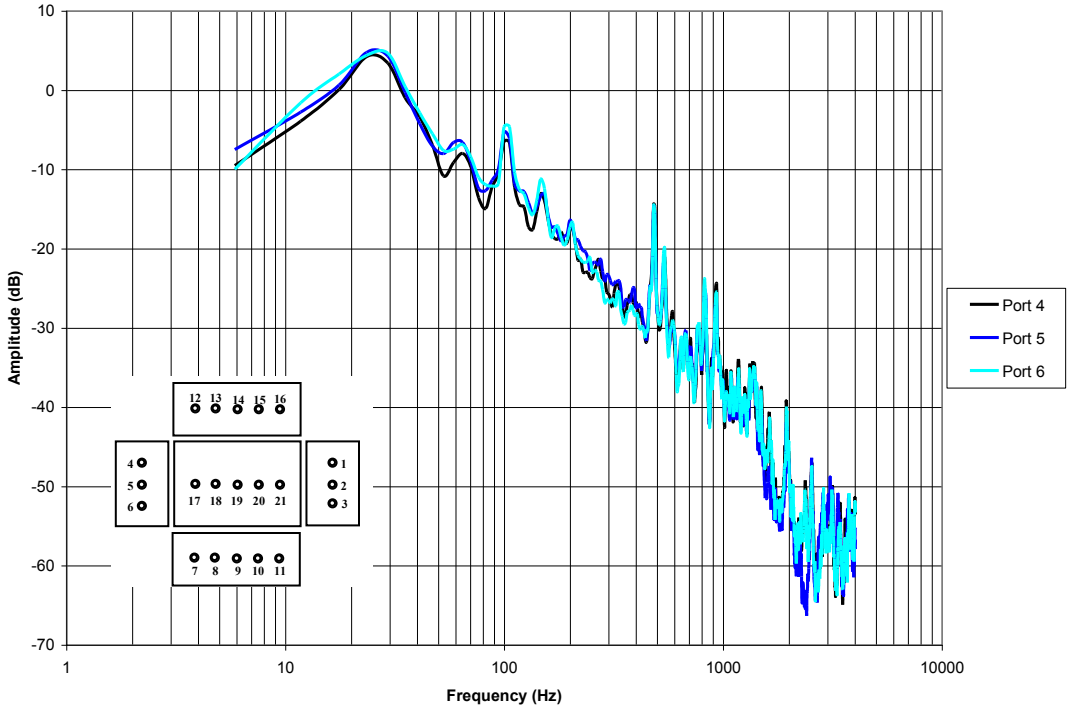

Figure 17: Cavity 2 microphone power spectra for Mach 0.05 at ports 4, 5, and 6.

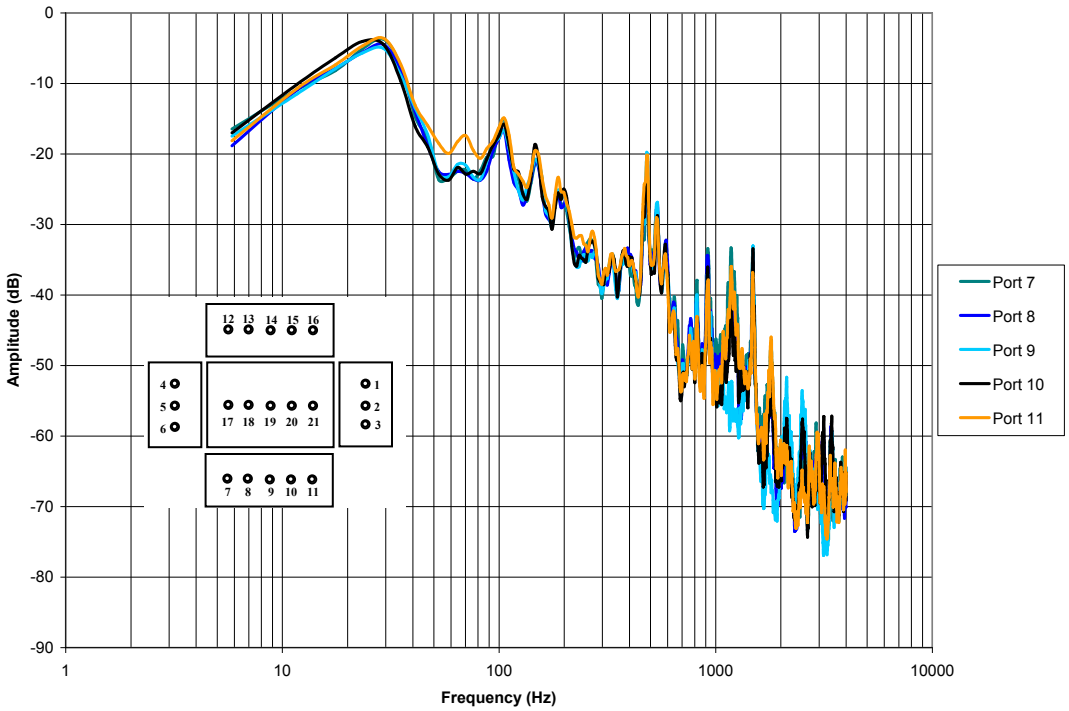

Figure 18: Cavity 2 microphone power spectra for Mach 0.05 at ports 7-11.

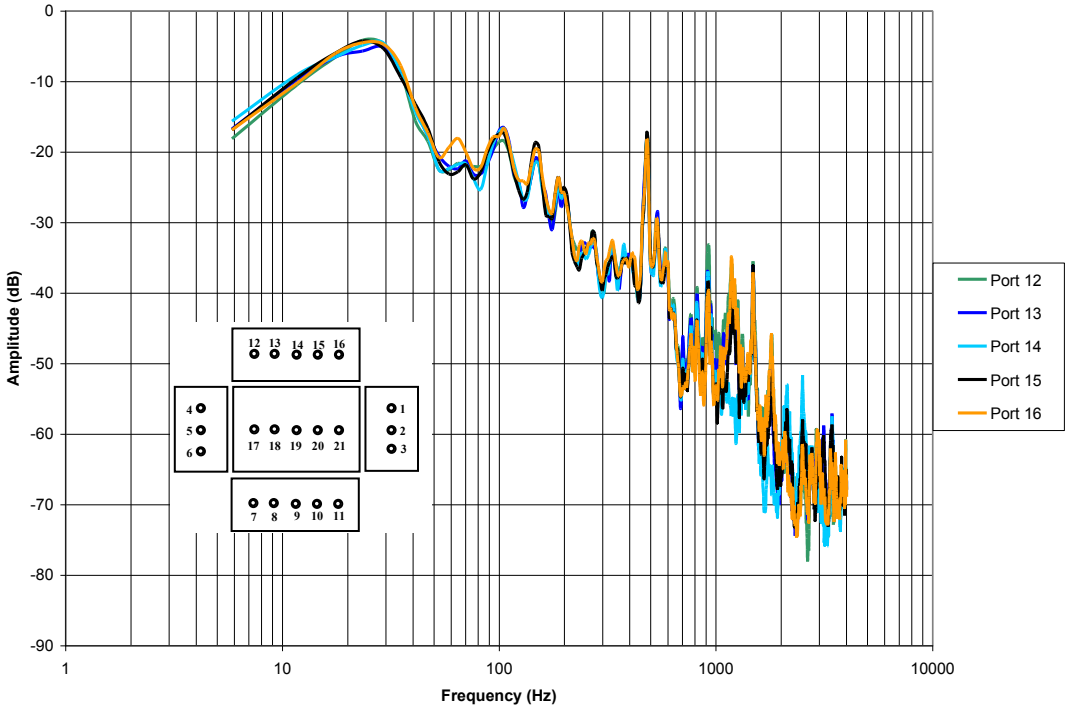

Figure 19: Cavity 2 microphone power spectra for Mach 0.05 at ports 12-16.

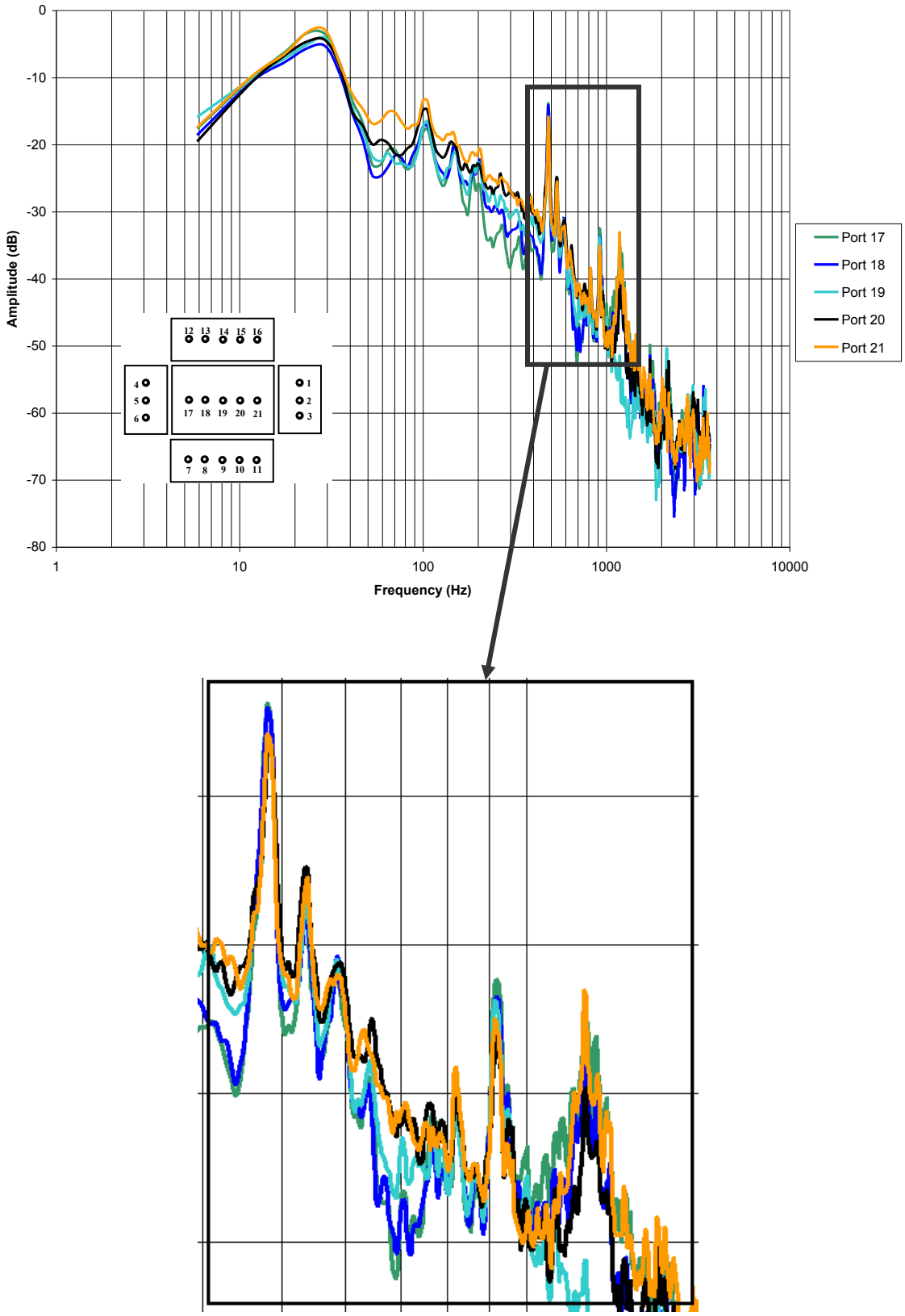

Figure 20: Cavity 2 microphone power spectra for Mach 0.05 at ports 17-21 with close-up view of largest amplitude peaks at high frequencies.

3.4 Confined Flow without Film

Confined flow tests were run for each cavity at varying Mach numbers (0.05-0.10) to determine if the resonance frequencies (1100 Hz to 3300 Hz) and the shear-layer frequencies (Rossiter modes) could be identified in the microphone power spectra. Figure 21 shows the Cavity 1 results. The highest sound level is in the lower frequency range. This is expected since the Mach number is low and the energy is low. These spectra are not shifted along the ordinate, so the largest amplitudes occur for higher Mach number as expected. However, the most significant peaks occur at the lower Mach numbers. In resonance, it is expected that the highest sound pressure levels would be at the higher Mach numbers with greater flow energy. According to the Rossiter equation, frequencies corresponding to the shear-layer modes should increase linearly with Mach number. Figure 22 shows a close-up from Figure 21 in the range of the expected shear-layer modes with dashed lines indicating the calculated Rossiter frequencies for modes 1 through 3. There is no evidence of mode 1 (25-50 Hz) or mode 3 (90-180 Hz). There is some indication of mode 2 in relatively small peaks from 60 to 100 Hz. However, the most significant peaks occur near 100 Hz over the Mach number range. This is far too small to be considered a resonance frequency which is expected to begin about 1100 Hz. Figure 23 shows a zoomed in view of Figure 21 in the higher frequency range to look for the resonant modes. Figure 23 shows three locations (highlighted by red dashed ovals) with significant peaks; the first is near 900 Hz, the second at 1700 Hz, and the third one at 2500 Hz. However, the peaks shrink as Mach number increases. While these frequencies are similar to the estimates for resonance frequencies, the greater flow energy

available at Mach number would indicate that the peaks should be growing. Results for Cavity 2 exhibit similar behavior as for Cavity 1, as shown in Figure 24. Figure 25 for the lower frequency range may indicate shear-layer mode 1 at slightly higher frequencies than the values computed by the Rossiter formula. Once again, there are significant peaks near 100 Hz across the Mach number range. Figure 26 for the higher frequency range shows possible resonant frequencies identified at 1200 Hz, 1700 Hz, and 3000 Hz, with dashed red ovals. Once again, these peaks shrink as the Mach number increases. Both cavities also exhibited peaks at 500-540 Hz that also decrease as Mach number increases. This could be noise from the motor or blower and as the flow increases, the sound in the cavity increases drowning out the noise from the motor.

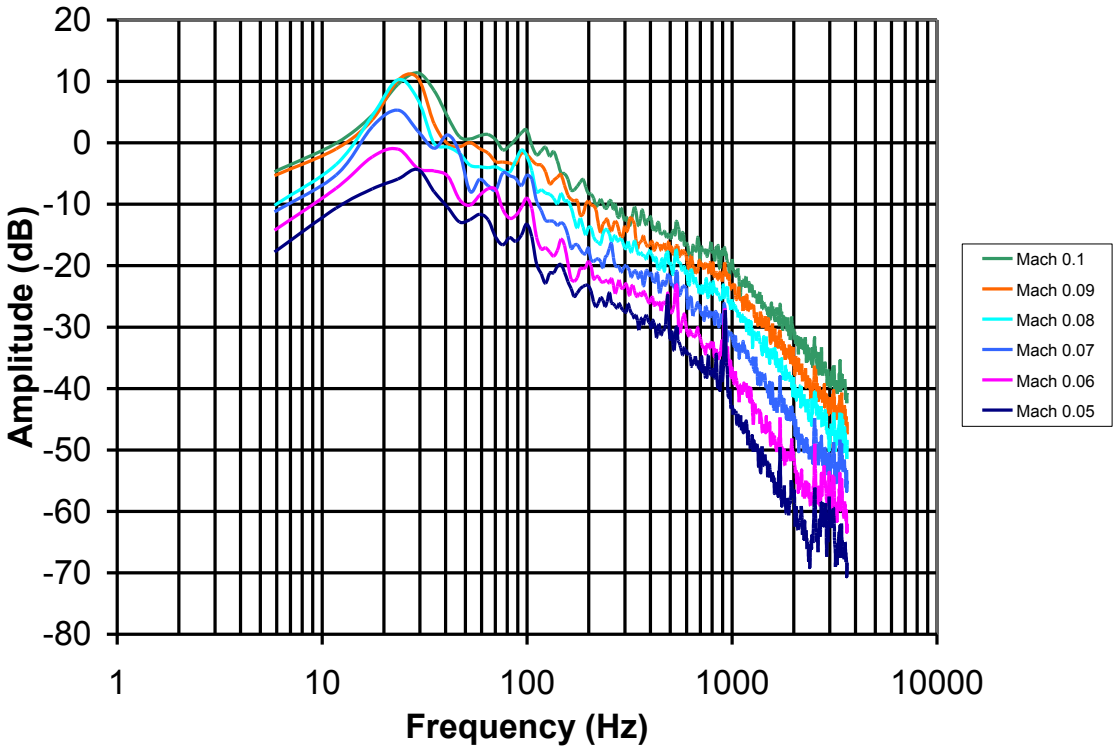

Figure 21: Cavity 1 microphone power spectra of confined flow at varying Mach numbers.

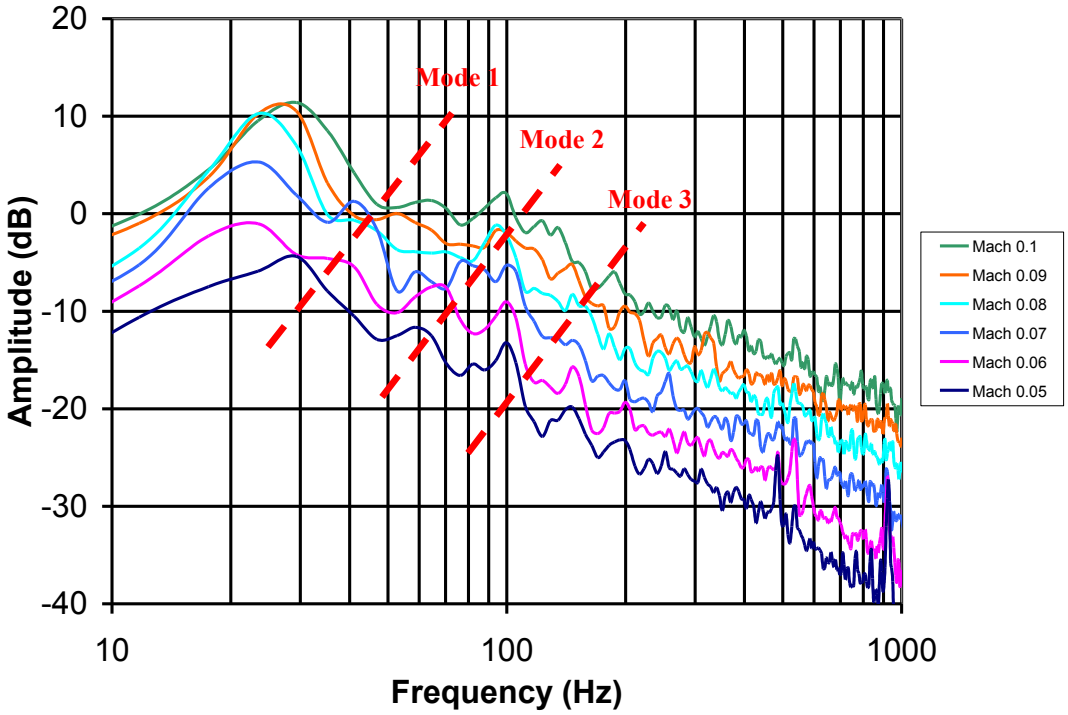

Figure 22: Cavity 1 microphone power spectra of confined flow at varying Mach numbers in the lower frequency range with red dashed lines indicating calculated Rossiter frequencies.

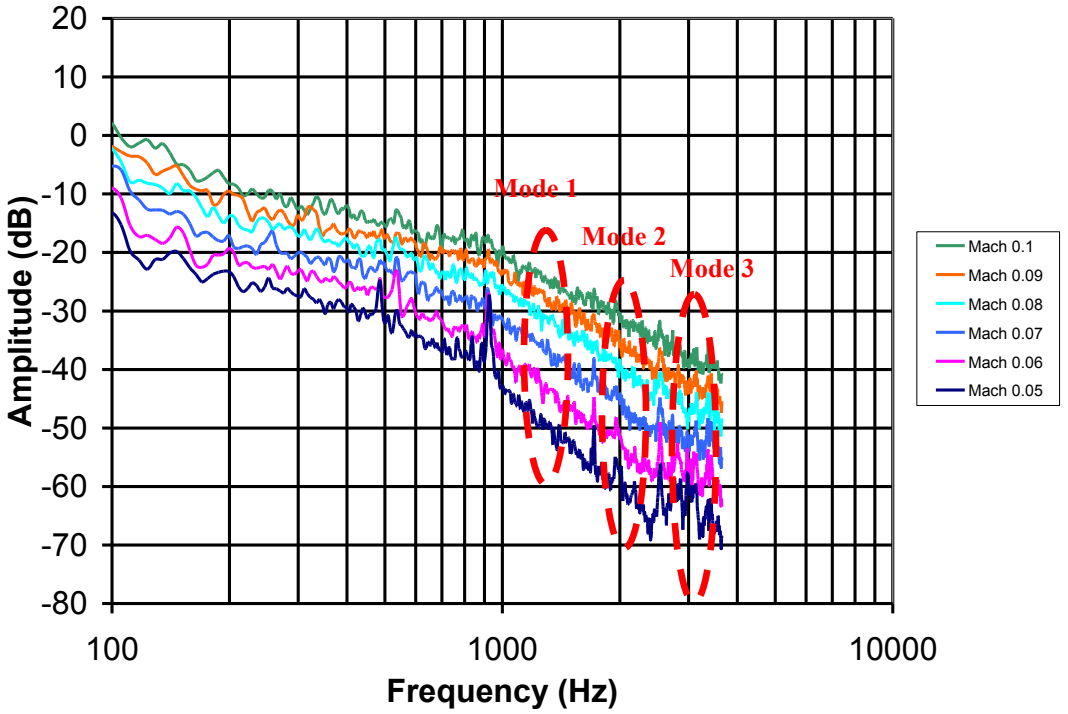

Figure 23: Cavity 1 microphone power spectra of confined flow at varying Mach numbers in the higher frequency range with red dashed ovals indicating peaks near resonance frequencies determined using the confinement ratio.

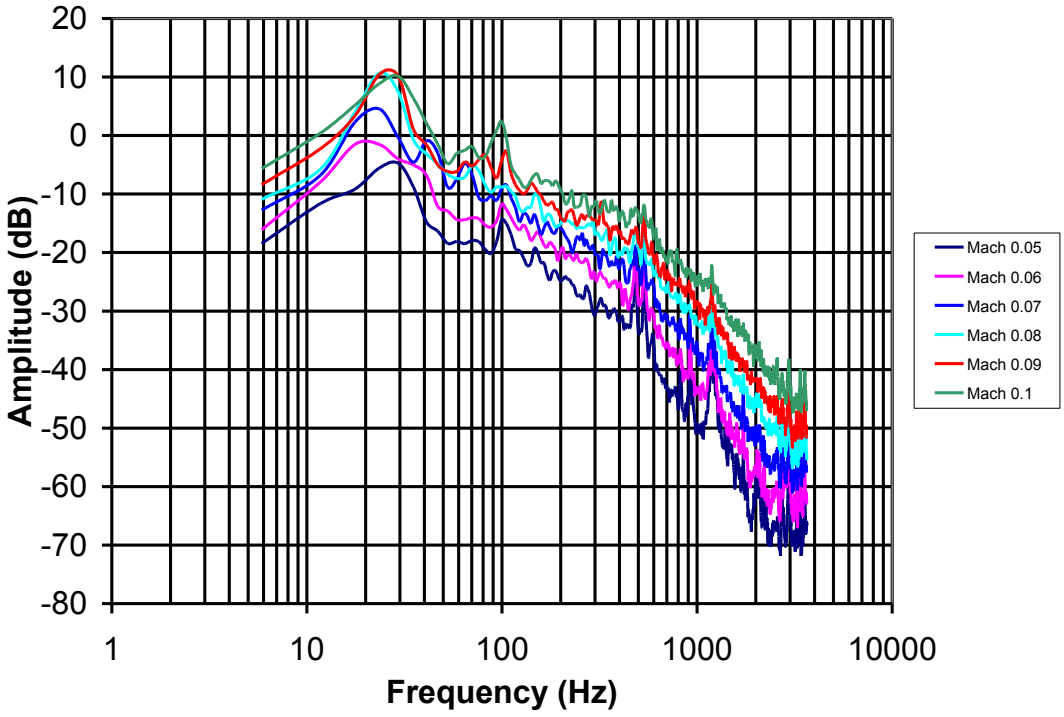

Figure 24: Cavity 2 microphone power spectra of confined flow at varying Mach numbers.

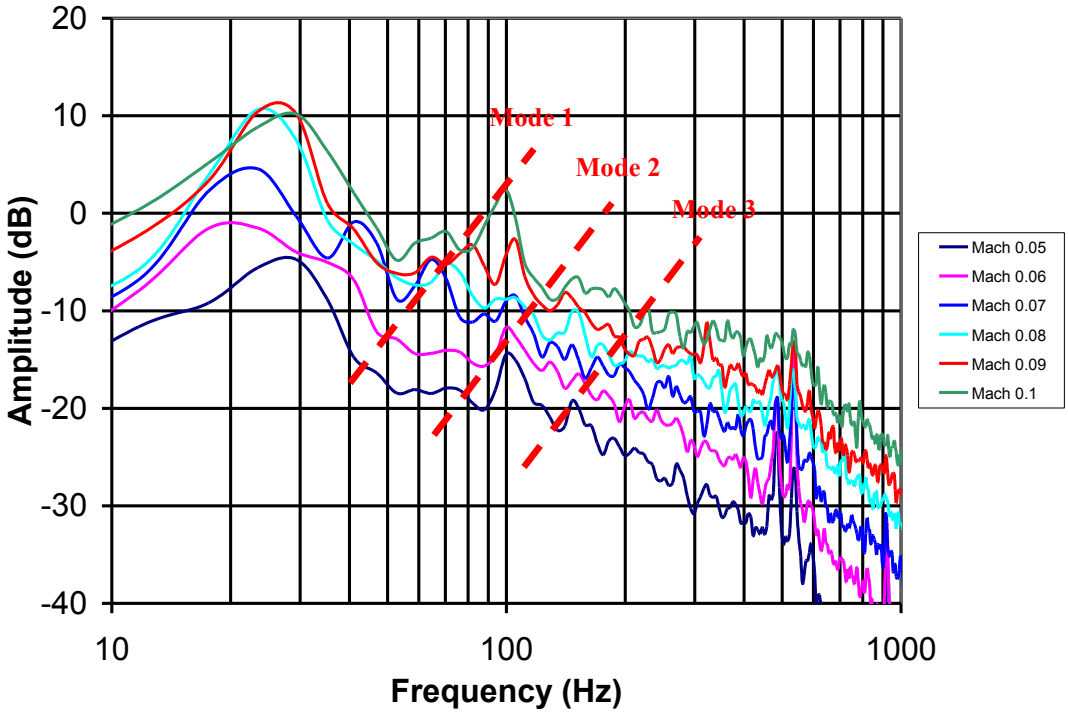

Figure 25: Cavity 2 microphone power spectra of confined flow at varying Mach numbers in the lower frequency range with red dashed lines indicating calculated Rossiter frequencies.

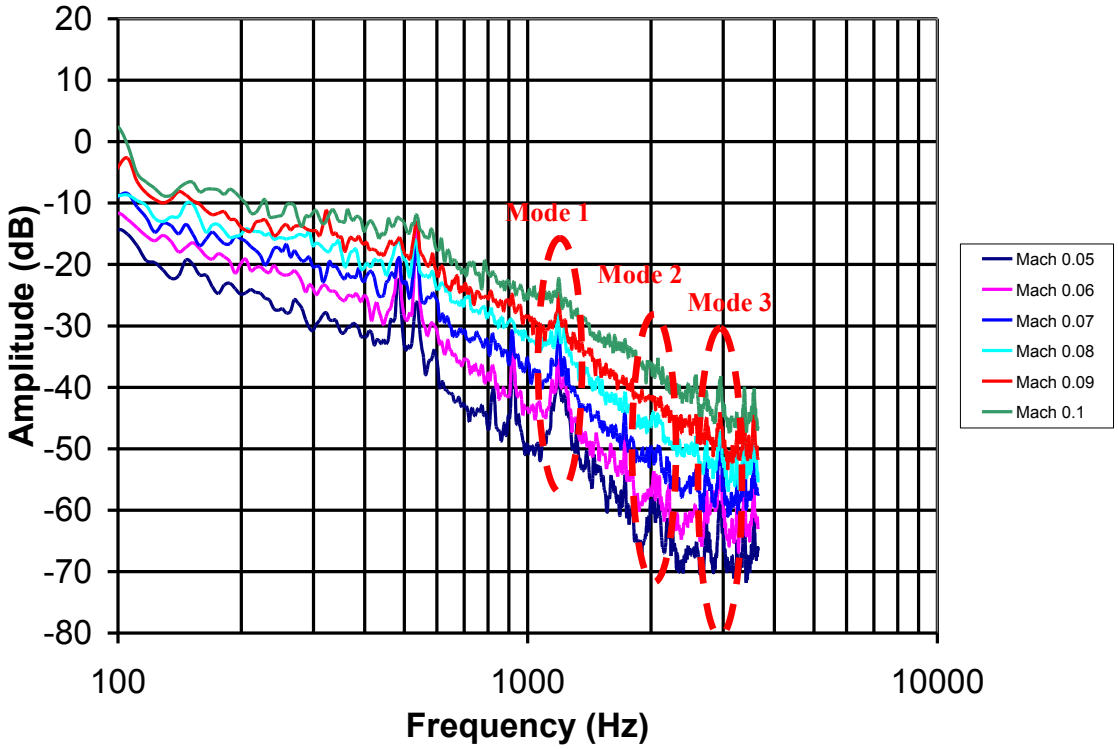

Figure 26: Cavity 2 microphone power spectra of confined flow at varying Mach numbers in the higher frequency range with red dashed ovals indicating peaks near resonance frequencies determined using the confinement ratio.

3.5 Determining Background Noise

Higher Mach numbers have more energy so the peaks should be highest. This was not seen in the low Mach number confined flow tests without film indicating that background noise may be the cause of the peaks. In an attempt to reduce background noise, additional tests were run using Styrofoam to plug each cavity with the microphone in the ports chosen in the previous section (port 27 in Cavity 1 and port 21 in Cavity 2 located downstream on the floor of the cavity). These tests were carried out to determine how background noise influenced the microphone measurements for cavity flows. This background may be produced by the blower or other components of the TBLG. The

cavities were removed from the window so that Styrofoam could be inserted in the cavity, plugging the cavity. The window with the cavity was placed back on the TBLG, and a test was run for each Mach number from 0.05 to 0.10 in increments of 0.01.

The acoustic software Audacity® has what is called a noise removal effect. This is used to remove unwanted sounds from a recording, e.g., people talking in the background during a speech. The user selects at least 1 second of sound they wish to remove (or noise) and in the Effects menu, Noise removal dialog, the user selects a button to indicate that the sound selected is noise. The user then selects the time series from which to remove this noise and determines how much of the noise they want filtered by using a slider bar with less filtering or more filtering. The degree of noise removal is not quantified. Minimal filtering was used initially. Figures 26 and 27 show the filtered and unfiltered microphone power spectra data for Cavity 1 and Cavity 2, respectively. Cavity 1 shows a large difference in Mach number ranges 0.08 to 0.10 where the noise recorded was significantly higher. The results for both cavities show that for lower Mach numbers, even this minimal filtering removed most of the signal especially for frequencies above about 500 Hz. The filtered signals show no improvement in identifying peaks associated with the shear-layer or resonance frequencies. Therefore, the noise removal function was not used.

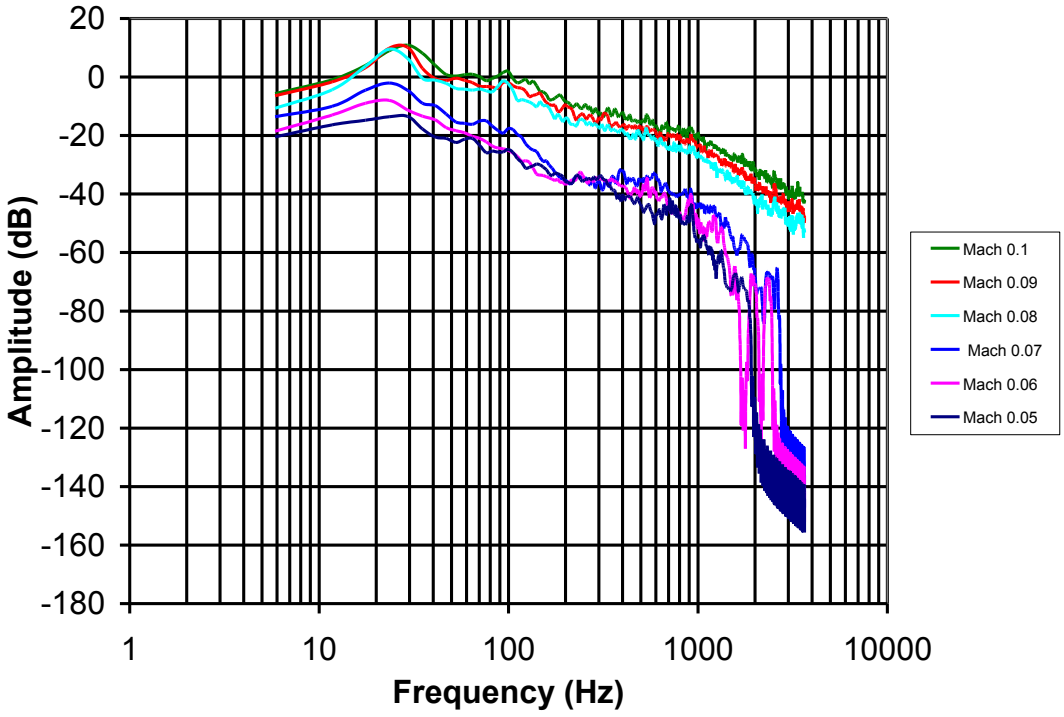

(a)

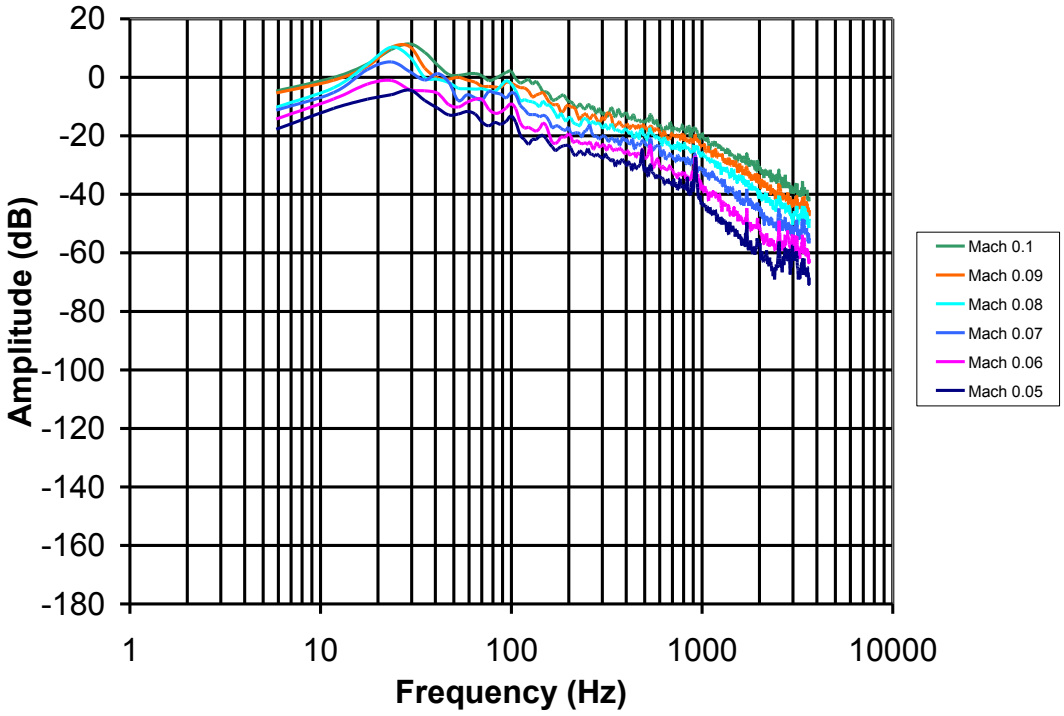

(b)

Figure 27: Cavity 1 microphone power spectra (a) with noise removal and (b) without noise removal.

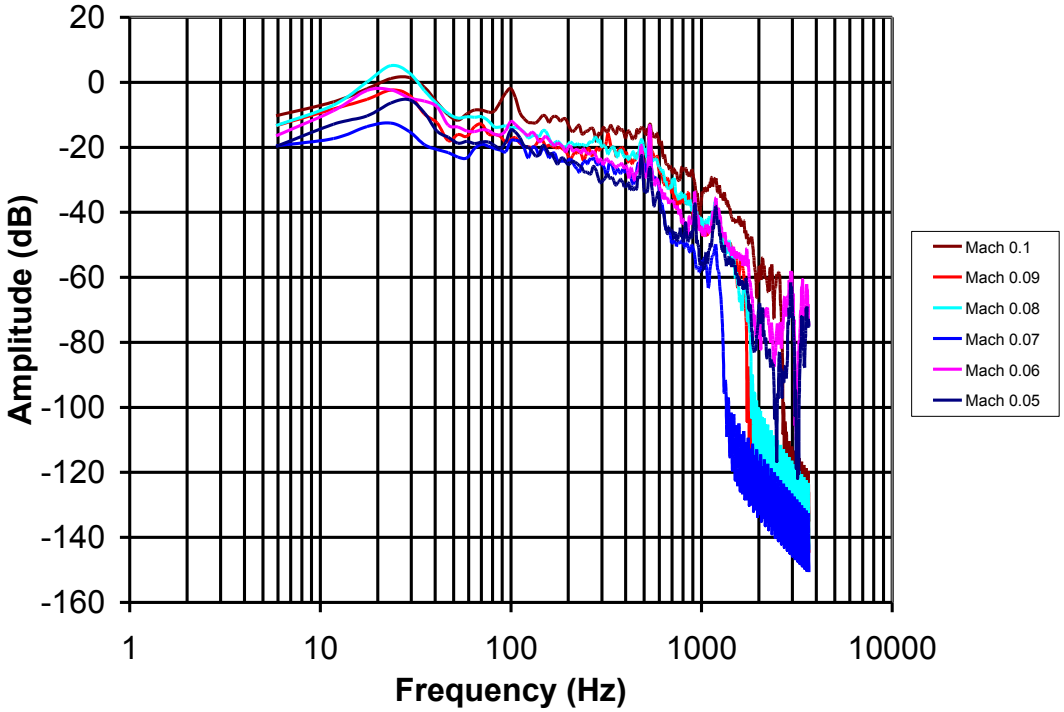

(a)

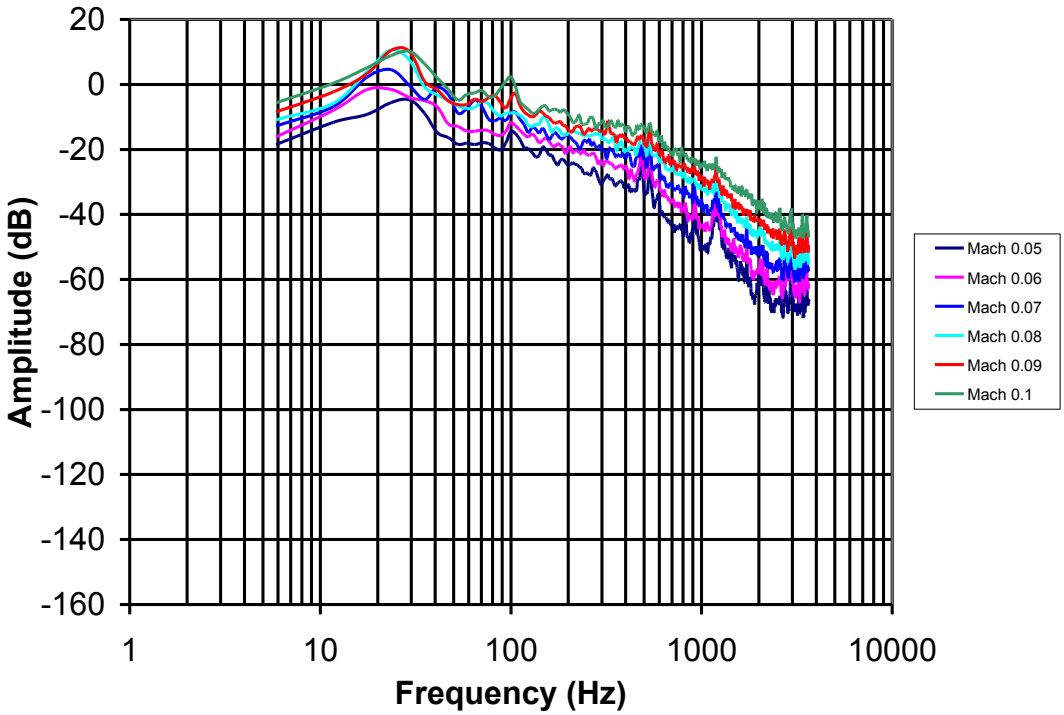

(b)

Figure 28: Cavity 2 microphone power spectra (a) with noise removal and (b) without noise removal.

3.6 Film Flutter Tests

Finally tests were run where the polymer film was placed on the mounting mechanism. The oscilloscope used to capture the vibrometer signal had a sampling rate set to 2MS/s or 2000 samples per second. The film was initially placed in the clamping device under no tension and tests were run at each Mach number. For the two subsequent tensions the film was replaced with new film. These results will be discussed in the next chapter.

CHAPTER 4

Effect of Film on Cavity Resonance

4.1 Results

Two different film tensions, 0.1 and 0.45 lbf, were tested for each cavity at varying Mach numbers and compared with the confined flow tests and tests with a film without tension. Figures 29-34 show the microphone power spectra for Cavity 1 at Mach numbers 0.05-0.10. Frequency ranges where peaks changed are indicated by red dashed ovals. Cavity 1 results show an increase in amplitude in all frequency ranges compared to the confined flow without film of 10-15 dB. Table 5 identifies frequencies at which peaks in the spectrum with no film present either increased or decreased in Cavity 1 tests. Although the peaks are not very significant, the film clearly has an effect on the cavity acoustics. The increased peaks are largely occurring in the frequency range of the shear-layer modes. For Mach 0.08 and Mach 0.09 the peak at 25 Hz decreases. The microphone power spectrum for Mach 0.08 is the only one not showing an increasing peak at 500 Hz. For Mach numbers 0.05 to 0.07, the spectra exhibit decreased peaks near the resonance frequency (1100 Hz) calculated from the mean height.

Cavity 1	Frequency (Hz)	
Mach number	Increased peaks	Decreased peaks
0.05	60, 550	100, 150, 500, 900, 1800
0.06	35, 70, 500	100, 150, 550, 900,1800
0.07	70, 500	900, 1800
0.08	45, 95	25
0.09	110, 250, 500	25
0.1	70, 500	25, 100

Table 5: Cavity 1 amplitude peaks at given frequencies.

Figures 35-40 show the microphone power spectra for Cavity 2 at Mach numbers 0.05-0.10. The results with the film appear to have higher amplitude as Mach number increased by as much as 3 dB. Again the peaks are not significant but indicate the film is having an effect on cavity acoustics. Table 6 lists frequencies at which peaks increased and decreased in comparison to Cavity 2 with no film. At Mach 0.10, the increased peaks are near the resonance frequencies 1100-3300 Hz. However for Mach 0.05-0.09, the peak nearest to the lowest resonance frequency (1100 Hz) decreases when the film is present.

Cavity 2	Frequency (Hz)	
Mach number	Increased peaks	Decreased peaks
0.05	-	100
0.06	70	100, 500, 550,1100
0.07	-	500,550, 1100
0.08	90, 250	500, 550, 1100
0.09	100,200	500, 550, 1100
0.1	1100, 2900	100, 200, 500

Table 6: Cavity 2 amplitude peaks at given frequencies.

Simultaneous laser vibrometer measurements on each film could not be obtained. The films stopped fluttering after each test began. It was observed that the film was pulled into the cavity and stabilized from the laser vibrometer data.

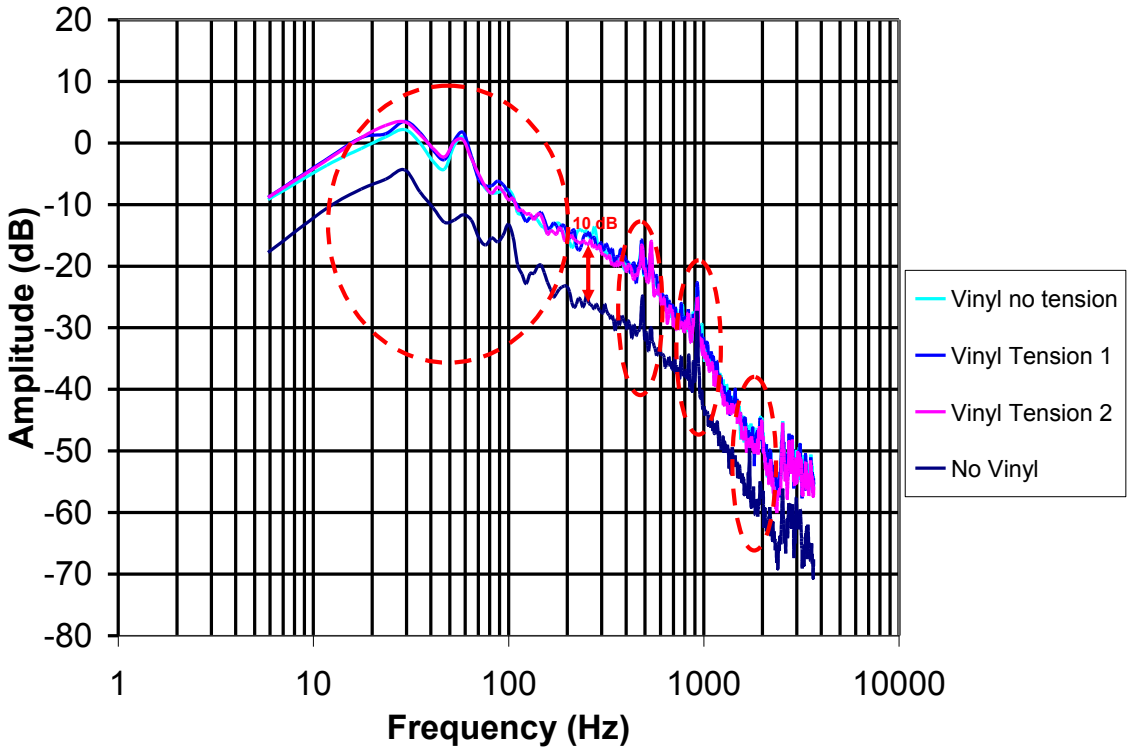

Figure 29: Cavity 1 microphone power spectra data at Mach 0.05 with film and without film.

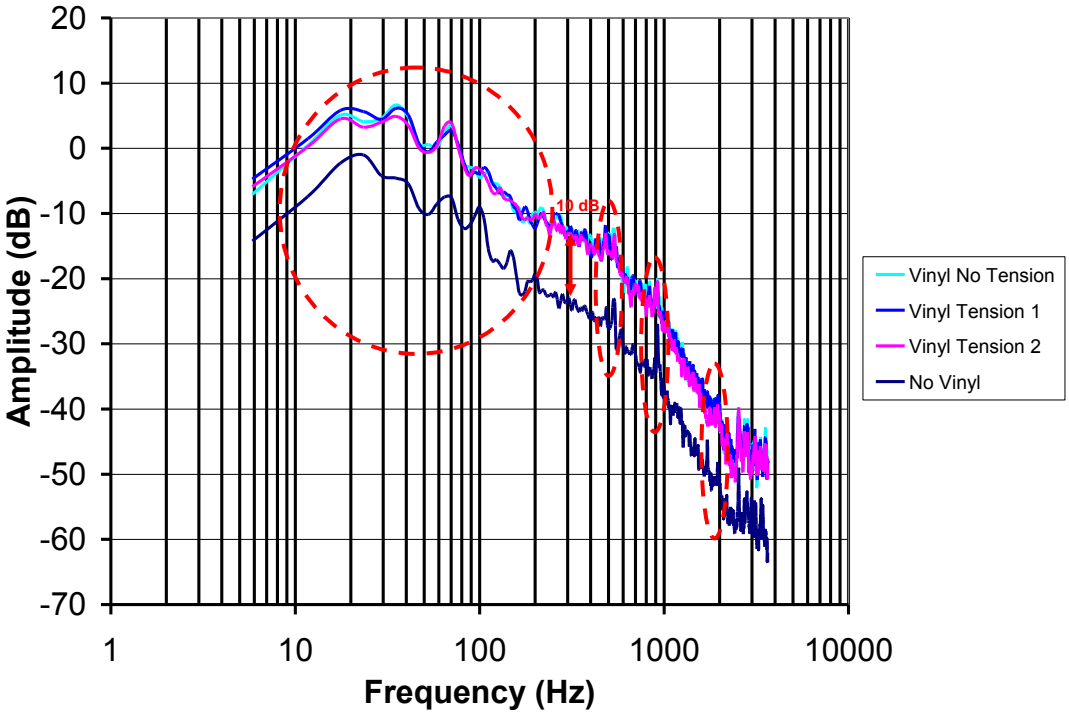

Figure 30: Cavity 1 microphone power spectra data at Mach 0.06 with film and without film.

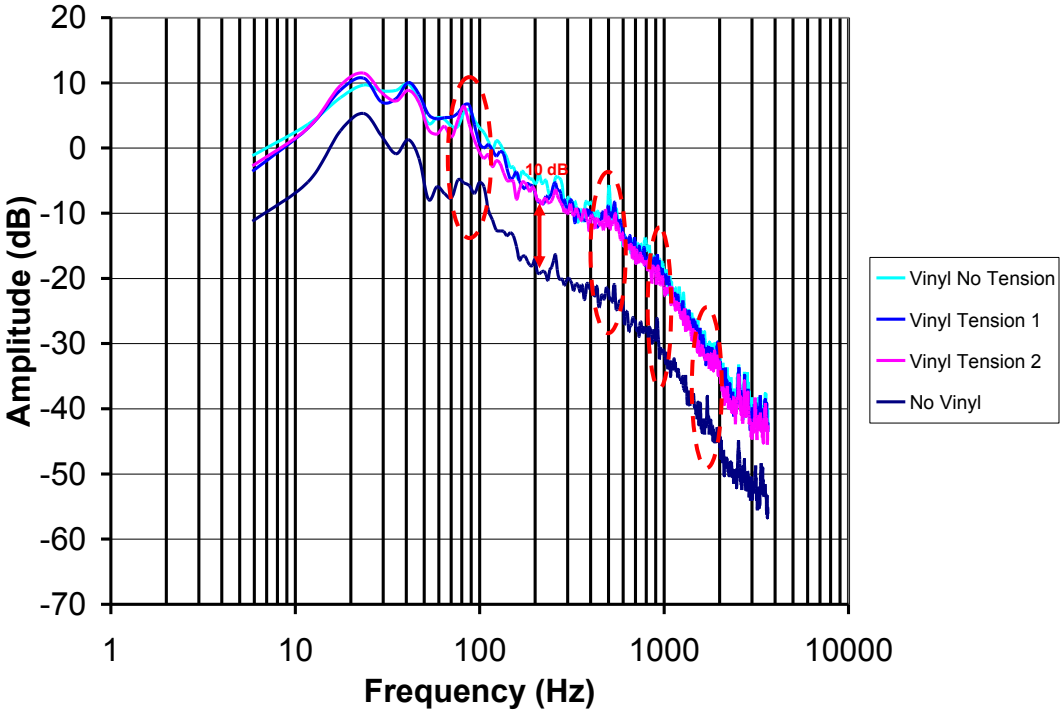

Figure 31: Cavity 1 microphone power spectra data at Mach 0.07 with film and without film.

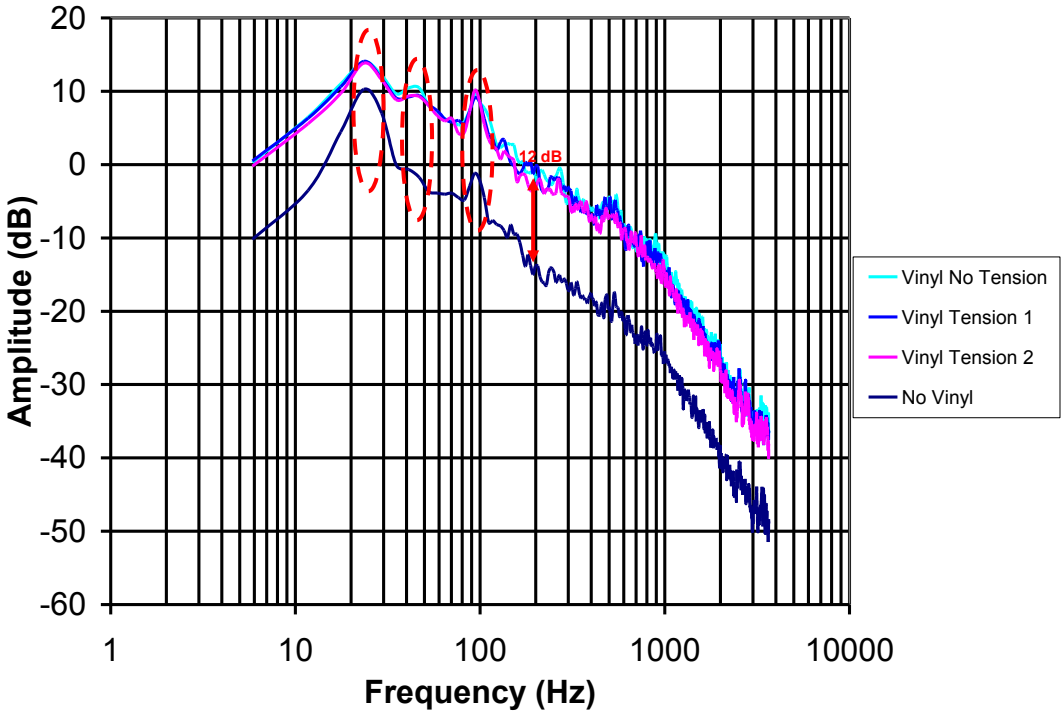

Figure 32: Cavity 1 microphone power spectra data at Mach 0.08 with film and without film.

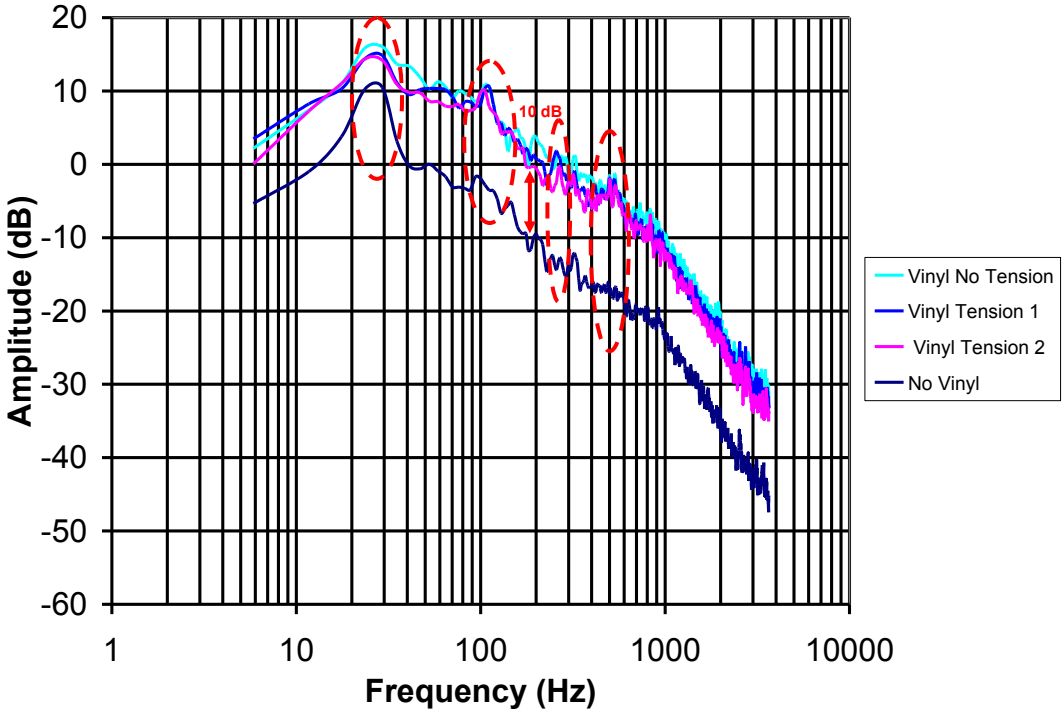

Figure 33: Cavity 1 microphone power spectra data at Mach 0.09 with film and without film.

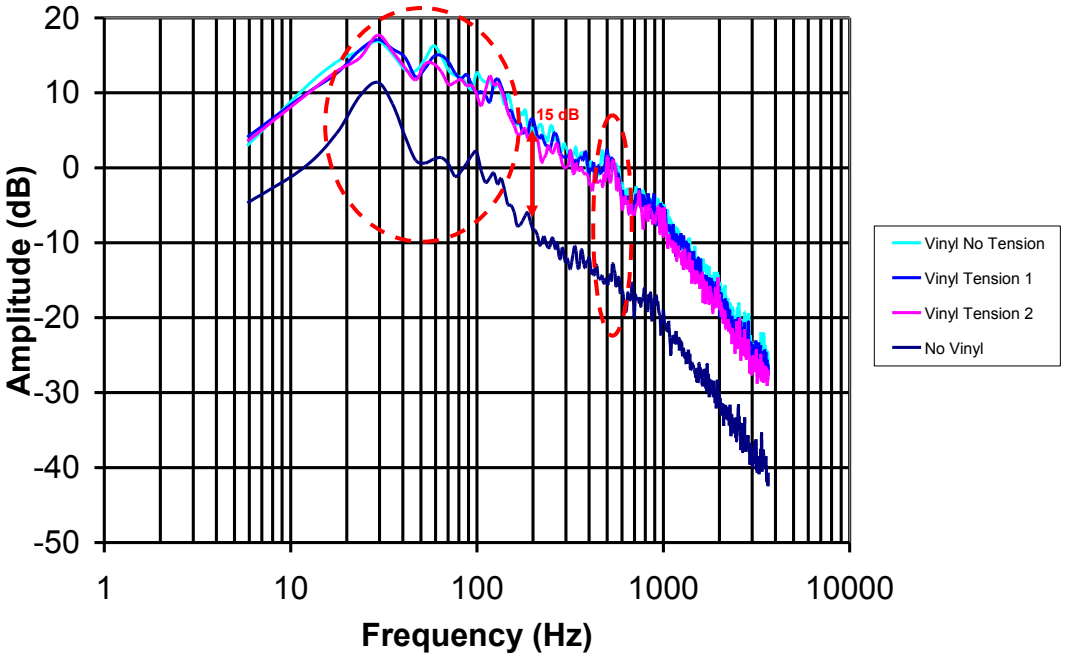

Figure 34: Cavity 1 microphone power spectra data at Mach 0.10 with film and without film.

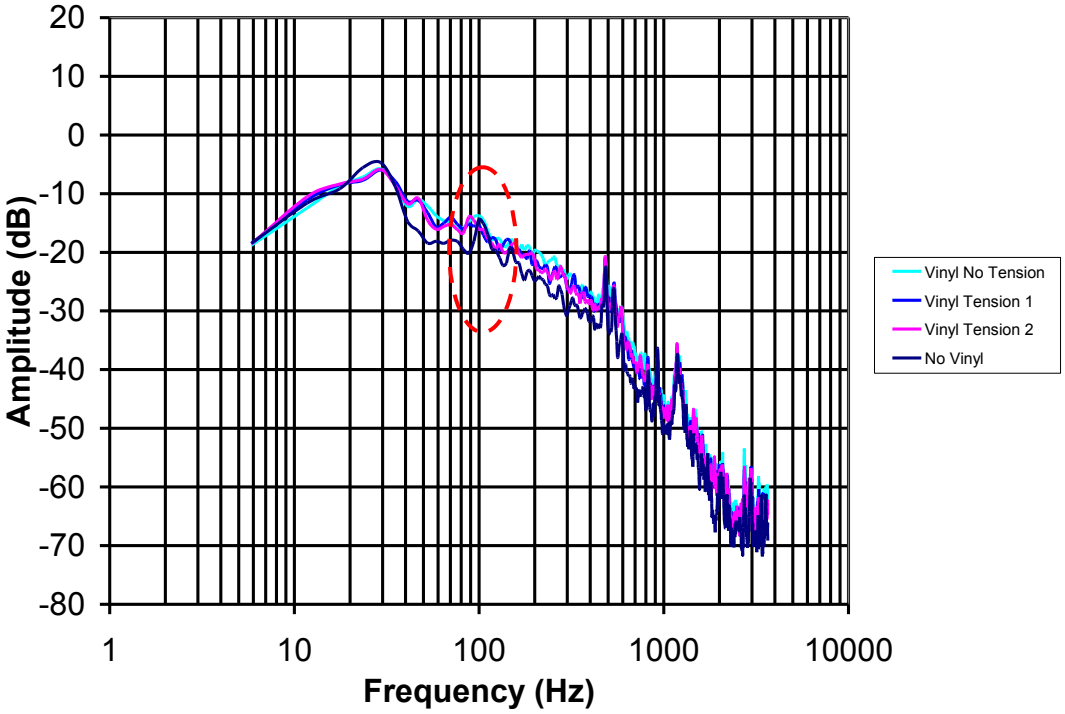

Figure 35: Cavity 2 microphone power spectra data at Mach 0.05 with film and without film.

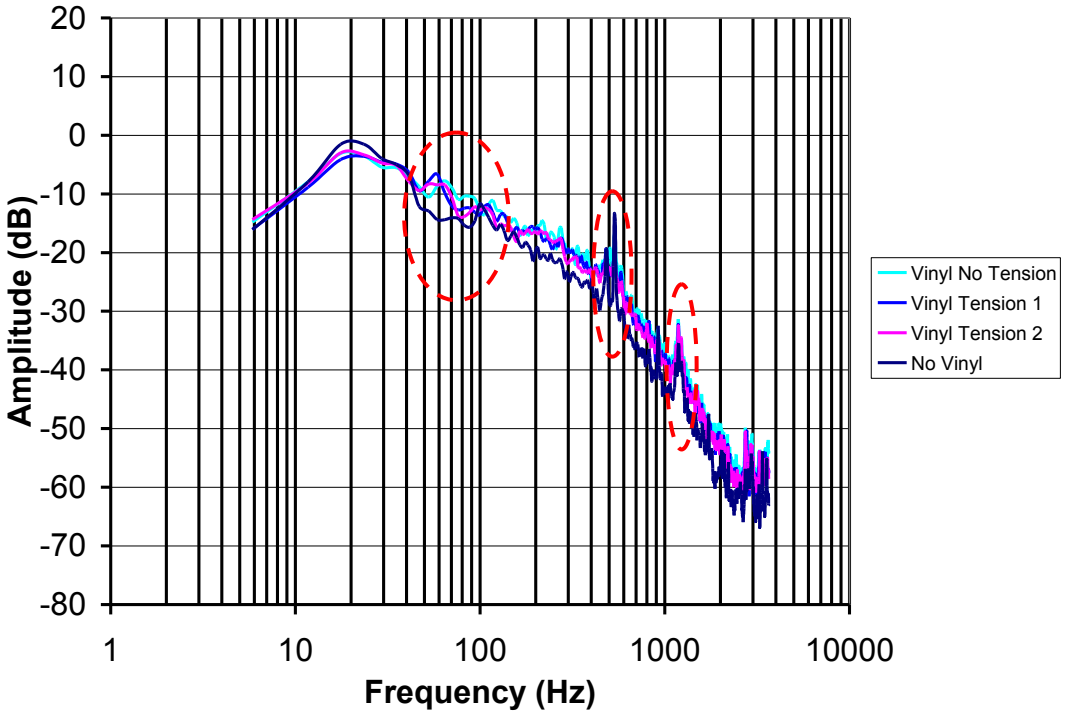

Figure 36: Cavity 2 microphone power spectra data at Mach 0.06 with film and without film.

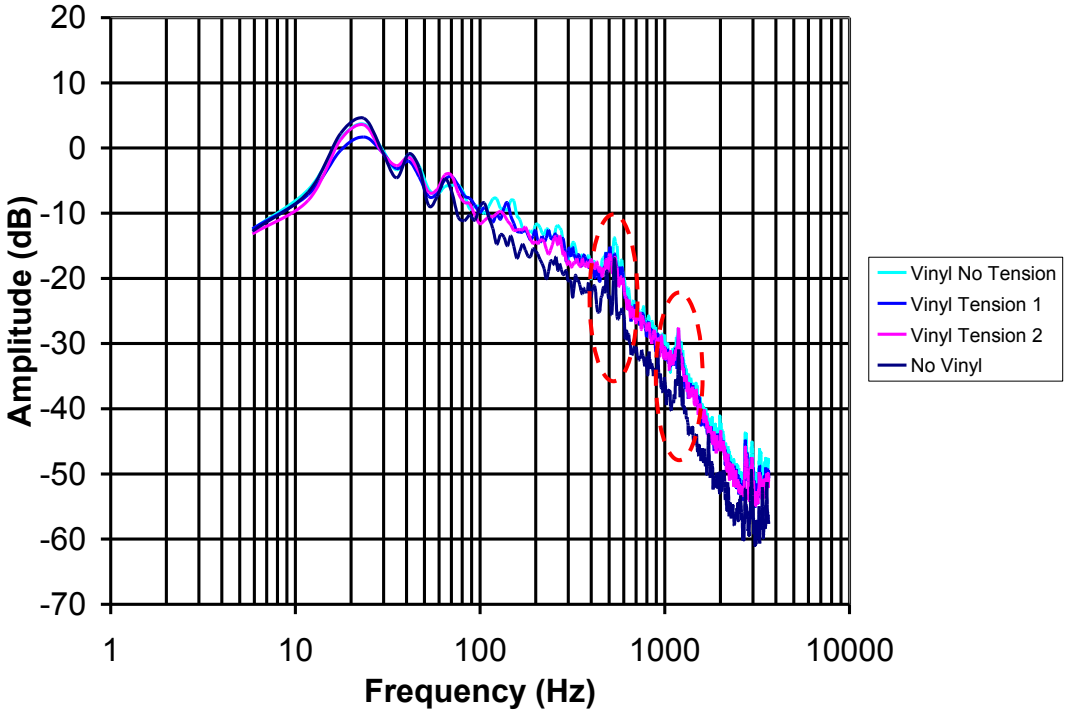

Figure 37: Cavity 2 microphone power spectra data at Mach 0.07 with film and without film.

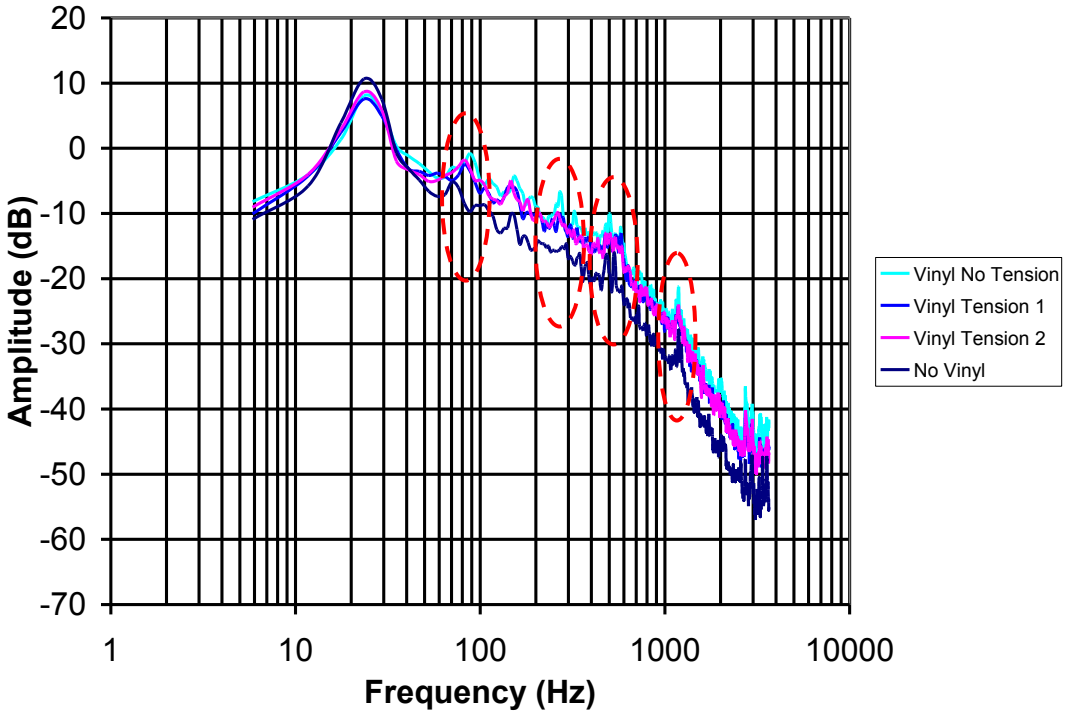

Figure 38: Cavity 2 microphone power spectra data at Mach 0.08 with film and without film.

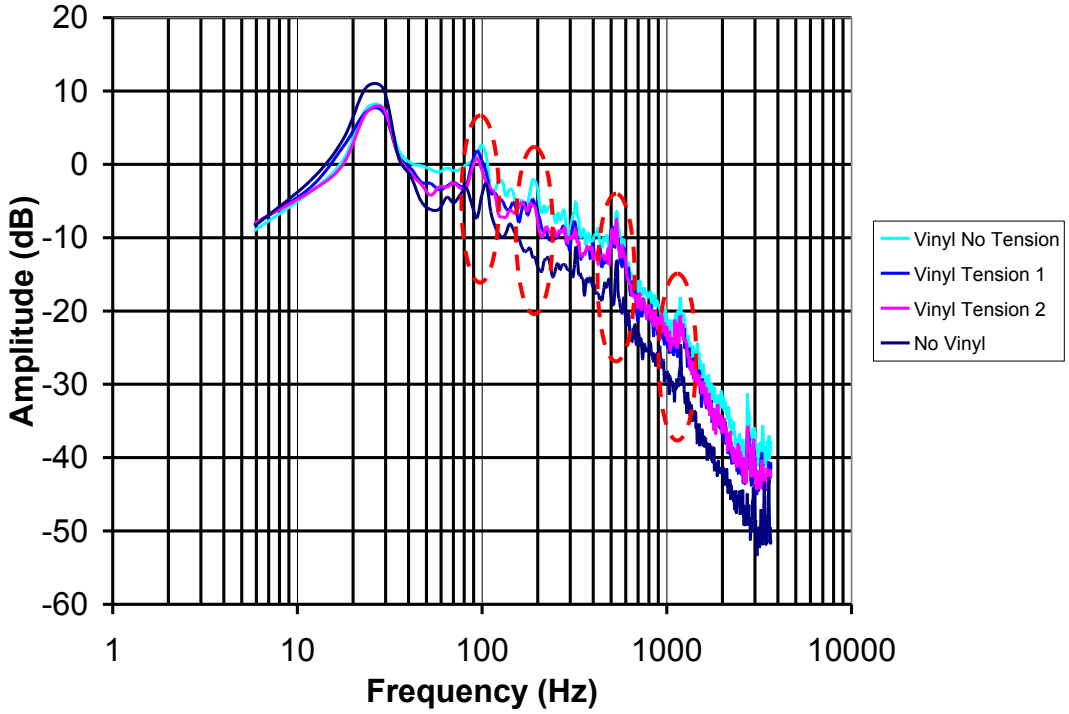

Figure 39: Cavity 2 microphone power spectra data at Mach 0.09 with film and without film.

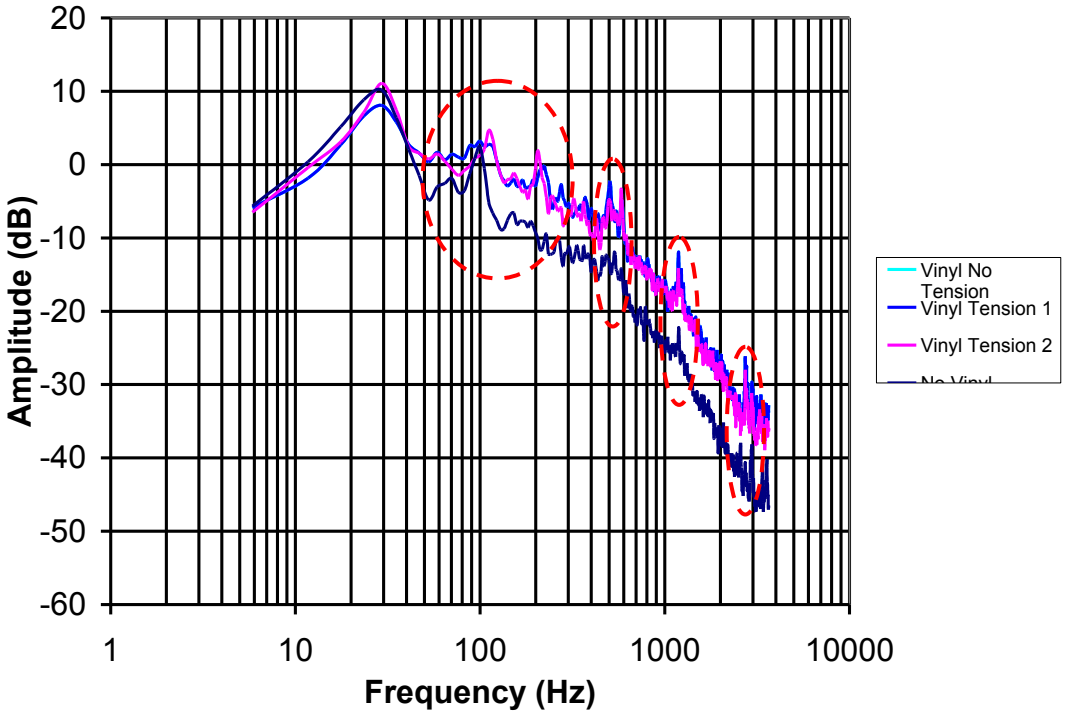

Figure 40: Cavity 2 microphone power spectra data at Mach 0.10 with film and without film.

4.2 Discussion

The power spectra for the microphone measurements without the film show that Cavity 2 has better resolved peaks than Cavity 1 and the same sound levels in the low frequency range (25-100 Hz). Both cavities exhibit peaks near 500 Hz and 1000 Hz at low Mach numbers. Cavity 2 at Mach 0.1 was the only test that had increasing peaks at 1100 Hz and 2900 Hz near the estimated mean height resonance modes. Mach 0.10 was the lower bound for Ziada et al. (2003) and was well below the flow speed at which shear-layer modes could be expected to excite their resonance modes. The increases with film present near the resonance modes are not observed for the shear-layer modes.

The size of the cavities and the mean height were significantly different than those reported by Ziada, et al. (2003) and could be part of the reason for not seeing resonance for Cavity 1 at lower Mach numbers. Because the present tests were performed at very low Mach numbers, the flow energy may be too low to produce these resonances.

Overall the film did seem to slightly affect the shear-layer resonances for both cavities. The major differences between Cavity 1 and Cavity 2 flows with films are in the sound levels compared to the confined flow with no film. Cavity 2 results are similar to the confined flow without the film while Cavity 1 shows significantly higher sound levels than the flow without film, with 10 – 15 dB differences. This significant difference could be due to the size of the film placed opposite the cavity. The film is longer than Cavity 2 by just 0.4 inches, but is shorter than Cavity 1 by 3 inches.

CHAPTER 5

Conclusion

5.1 Conclusion

Two open, shallow cavities were designed and tested in confined flow at very low Mach numbers. A tensioned polymer film was placed opposite the cavity in a wind tunnel where its flutter could possibly excite or dampen the resonant frequencies. An attempt was made to use a laser Doppler vibrometer to measure the film flutter velocity. However, there was no flutter because the film was pulled into static deflection. The only difference between the cavities was their length compared to the length of the film. The film was shorter than Cavity 1 and slightly longer than Cavity 2. Cavity 1 (L/D =2.5) microphone power spectra showed larger pressure oscillations across all frequencies for all Mach numbers from 0.05 to 0.10 compared to confined flows with no film. Cavity 2 (L/D=1.5) microphone power spectra with and without the film showed an increase of 3 dB at Mach 0.10. The film did affect the shear-layer frequencies in cavities, dampening and exciting them. Cavity 2 showed two increasing peaks (1100 Hz and 2900 Hz) at Mach 0.10 near the estimated resonance frequencies of 1100-3300 Hz.

5.2 Implications for Future Work

The film clamping mechanism could be designed to fit inside the cavity closer to the source of shear-layer oscillations. This may improve the film flutter interaction with the cavity oscillations. Because the length of the film made a significant difference in the

sound amplitude the film should also be shorter and rotated 90°. Various film thicknesses and types should also be tested. Reflective films will also improve the laser Doppler vibrometer measurements by increasing reflection from the fluttering film. Different cavity sizes including different depths should also be tested.

REFERENCES

Ahuja, K. K., and Mendoza, J., Effect of cavity dimensions, boundary layer, and temperature on cavity noise with emphasis to benchmark data to validate computational aeroacoustic codes, NASA Contractor Report CR-4653 (1995).

Alvarez, J. O., Kerschen, E. J., and Tumin, A., A theoretical model for cavity acoustic resonances in subsonic flow, AIAA Paper 2004-2845 (2004).

Blackstock, D.T., *Fundamentals of physical acoustics*. New York: A Wiley-Interscience Publication John Wiley & Sons.

Cattafesta III, L. N., Song, Q., Williams, D. R., Rowley, C. W., Alvi, F. S., Active control of flow-induced cavity oscillations, *Progress in Aerospace Sciences* (2008), 44:479-502.

Dix, R. E., and Bauer, R. C., Experimental and predicted acoustic amplitudes in a rectangular cavity, AIAA Paper 2000-0472 (2000).

Faure, T. M., Adrianos, P., Lusseyran, F., and Pastur, L., Visualizations of the flow inside an open cavity at medium range Reynolds numbers, *Experiments in Fluids* (2007), 42:169–184.

Kistler, A. C., and Tan, F. C., Some properties of turbulent separated flows, *The Physics of Fluids Supplement: Boundary Layers and Turbulence* (1967), 10(9):S165–173.

Koch, W., Acoustic resonances in rectangular open cavities, *AIAA Journal* (2005), 43(11): 2342-2349.

Lamp, A. M., and Chokani, N., Computation of cavity flows with suppression using jet blowing, *Journal of Aircraft* (1997), 34(4):545-51.

Lin, J. C., and Rockwell, D., Organized oscillations of initially turbulent flow past a cavity, *AIAA Journal* (2001), 39(6):1139-1151.

Maull, D. J., and East, L. F., Three-dimensional flow in cavities, *Journal of Fluid Mechanics* (1963), 16:620–632.

Plentovich, E., Three–dimensional cavity flow fields at subsonic and transonic speeds, NASA Technical Memorandum TM 4209 (1992).

Plumblee, H., Gibson,J., and Lassiter,L., A theoretical and experimental investigation of the aeroacoustic response of cavities in aero-dynamic flow, WADD-TR-61-75,Wright–Patterson AFB, Dayton, OH (1962).

Rockwell, D., and Knisely, C., Observations of the three–dimensional nature of unstable flow past a cavity, *Physics of Fluids* (1980), 23:425–431.

Rockwell, D., and Naudascher,E., Review—self-sustaining oscillations of flow past cavities, *Journal of Fluids Engineering* (1978), 100:152-165.

Rossiter, J. E., Wind tunnel experiments on the flow over rectangular cavities at subsonic and transonic speeds, *Royal Aircraft Establishment*, Technical Report 64037 (1964).

Rowley, C. W., Colonius, T., and Basu, A. J., On self-sustained oscillations in two-dimensional compressible flow over rectangular cavities, *Journal of Fluid Mechanics* (2002), 455:315–346.

Rowley, C. W., Juttijudata,V., and Williams, D. R., Cavity flow control simulations and experiments, 43rd Aerospace Sciences Meeting and Exhibit, Reno, NV, AIAA Paper 2005-0292 (2005).

Sarohia V., and Massier, P. F., Control of cavity noise, *Journal of Aircraft* (1977), 14(9):833-7.

Tam, C. K. W., and Block, P. J. W., On the tones and pressure oscillations induced by flow over rectangular cavities, *Journal of Fluid Mechanics* (1978), 89:373-399.

Ziada, S., Ng, H., Blake, C. E., Flow excited resonance of a confined shallow cavity in low Mach number flow and its control, *Journal of Fluids and Structures* (2003), 18:79-92.